AD-A039 055 NIELSEN ENGINEERING AND RESEARCH INC MOUNTAIN VIEW CALIF F/G 20/4
RESEARCH ON UNSTEADY TRANSONIC FLOW THEORY.(U)
APR 76 S S STAHARA, J R SPREITER N00014-73-C-0379
UNCLASSIFIED NEAR-TR-132 NL

| OF |
AD
A039055

END

DATE
FILMED
5-77

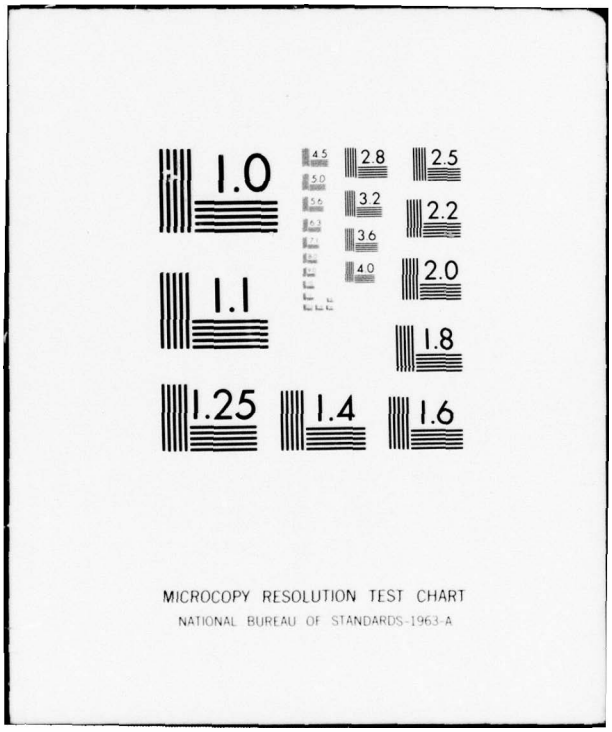
1.0
1.1
1.25
1.4
1.6
1.8
2.0
2.2
2.5
2.8
3.2
3.6
4.0
4.5
5.0
5.6
6.3
MICROCOPY RESOLUTION TEST CHART
NATIONAL BUREAU OF STANDARDS-1963-A

12

NIELSEN ENGINEERING
AND RESEARCH, INC.

OFFICES: 510 CLYDE AVENUE / MOUNTAIN VIEW, CALIFORNIA 94043 / TELEPHONE (415) 968-9457

COPY NO. 9

RESEARCH ON UNSTEADY TRANSONIC FLOW THEORY

by

Stephen S. Stahara and John R. Spreiter

NEAR TR 132

April 1977

Prepared under Contract No. N00014-73-C-0379

by

NIELSEN ENGINEERING & RESEARCH, INC.
Mountain View, California

for the

OFFICE OF NAVAL RESEARCH
Arlington, Virginia

UNCLASSIFIED

SECURITY CLASSIFICATION OF THIS PAGE (When Data Entered)

REPORT DOCUMENTATION PAGE		READ INSTRUCTIONS BEFORE COMPLETING FORM
1. REPORT NUMBER	2. GOVT ACCESSION NO.	3. RECIPIENT'S CATALOG NUMBER
4. TITLE (and Subtitle) Research on UNSTEADY TRANSONIC FLOW THEORY.		5. TYPE OF REPORT & PERIOD COVERED Technical Report.
		6. PERFORMING ORG. REPORT NUMBER NEAR-TR-132
7. AUTHOR(s) Stephen S. Stahara and John R. Spreiter		8. CONTRACT OR GRANT NUMBER(s) N00014-73-C-0379
9. PERFORMING ORGANIZATION NAME AND ADDRESS Nielsen Engineering & Research, Inc. 510 Clyde Avenue Mountain View, California 94043		10. PROGRAM ELEMENT, PROJECT, TASK AREA & WORK UNIT NUMBERS NR 061-215
11. CONTROLLING OFFICE NAME AND ADDRESS Office of Naval Research Code 438, Department of the Navy Arlington, Virginia 22217		12. REPORT DATE April 1976
		13. NUMBER OF PAGES 34
14. MONITORING AGENCY NAME & ADDRESS(if different from Controlling Office) Office of Naval Research Code 438, Department of the Navy Arlington, Virginia 22217		15. SECURITY CLASS. (of this report) Unclassified
		15a. DECLASSIFICATION/DOWNGRADING SCHEDULE N/A

16. DISTRIBUTION STATEMENT (of this Report)

Reproduction in whole or in part is permitted for any purpose of the United States Government. Approved for public release; distribution unlimited.

17. DISTRIBUTION STATEMENT (of the abstract entered in Block 20, if different from Report)

34 pp.

18. SUPPLEMENTARY NOTES

N/A

19. KEY WORDS (Continue on reverse side if necessary and identify by block number)

Transonic Flow
Unsteady Flow
Bodies of Revolution
Stability Derivatives

CONTENTS!

20. ABSTRACT (Continue on reverse side if necessary and identify by block number)

This report consists of three papers, "Unsteady Local Linearization Solution for Pulsating Bodies at $M_\infty = 1$" by S. S. Stahara and J. R. Spreiter, AIAA Journal, vol. 14, July 1976, pp. 990-992, "Unsteady Local Linearization Solution for Pitching Bodies of Revolution at $M_\infty = 1$: Stability Derivative Analysis" by S. S. Stahara and J. R. Spreiter, AIAA Journal, vol. 14, October 1976, pp. 1402-1408, and "Developments in

DD FORM 1 JAN 73 1473 EDITION OF 1 NOV 65 IS OBSOLETE

UNCLASSIFIED

SECURITY CLASSIFICATION OF THIS PAGE (When Data Entered)

20. Transonic Steady and Unsteady Flow Theory," by J. R. Spreiter and S. S. Stahara, Proceedings of the 10th Congress of the International Council of the Aeronautical Sciences (ICAS), October 1974, pp. 100-114.

Preface

This report consists of three papers describing research on unsteady transonic flow theory. The first, entitled "Unsteady Local Linearization Solution for Pulsating Bodies at $M_\infty = 1$", by S. S. Stahara and J. R. Spreiter has been published in the AIAA Journal, vol. 14, July 1976, pp. 990-992. The second, entitled "Unsteady Local Linearization Solution for Pitching Bodies of Revolution at $M_\infty = 1$: Stability Derivative Analysis", by S. S. Stahara and J. R. Spreiter has been published in the AIAA Journal, vol. 14, October 1976, pp. 1402-1408. The third publication is ICAS Paper No. 76-06, entitled "Developments in Transonic Steady and Unsteady Flow Theory", by J. R. Spreiter and S. S. Stahara. This paper was presented by Professor J. R. Spreiter at the 10th Congress of the International Council of the Aeronautical Sciences (ICAS) in Ottawa, Canada, October 3-8, 1976.

These papers are based on research carried out under Contract No. N00014-73-C-0379, Project No. NR 061-215 sponsored by the Office of Naval Research with Mr. Morton Cooper as Technical Monitor.

Unsteady Local Linearization Solution for Pulsating Bodies at $M_\infty = 1$

Stephen S. Stahara*
Nielsen Engineering & Research, Inc., Mountain View, Calif.
and
John R. Spreiter†
Stanford University, Stanford, Calif.

Introduction

WITH the continuing development of successful techniques for solving steady transonic flows, considerable interest has been focused recently on the development of methods to solve unsteady transonic problems.[1] In this note we describe the local linearization solution for transonic flow past slender bodies of revolution undergoing oscillatory pulsatile motion of the body surface. This result provides the fundamental unsteady source solution from which higher-order multipole solutions (dipole, etc.) necessary to describe more complex unsteady motions (e.g., translation, rotation) can be obtained. The theory is based on the concept of dividing the flow into steady and unsteady components and solving the resultant equations by the local linearization method.[2] The analysis is developed generally for sonic and near sonic flows, with specific applications made to parabolic-arc half-bodies and cones at freestream Mach number $M_\infty = 1$. The results indicate the correct convergence to nonlinear quasisteady theory as the reduced frequency of oscillation based on body length, $k \to 0$, and to linear acoustic theory as k becomes large ($k \geq 1$). For $k \leq 1$, a range of prime importance in many flutter and stability applications, the unsteady solutions exhibit a significant nonlinear thickness effect induced by the steady-state solution, much like that displayed in the two-dimensional case.[3] This indicates a basic shortcoming of linear theory in this frequency range.

Analysis

The concept that a major body of transonic flow problems can be predicted accurately within the framework of inviscid, nonlinear small-disturbance theory, described by the equation

$$(1-M_\infty^2)\phi_{xx} + \phi_{rr} + \frac{1}{r}\phi_r + \frac{1}{r^2}\phi_{\theta\theta} = M_\infty^2(\gamma+1)\phi_x\phi_{xx} + M_\infty^2\phi_{tt} + 2M_\infty^2\phi_{xt} \tag{1}$$

has been well-established.[4,5] In Equation (1), M_∞ is the freestream Mach number; (x,r,θ) are nondimensional body-fixed cylindrical coordinates with (x,r) normalized by body length ℓ and with the x-axis directed rearward and aligned with the body centerline; t is nondimensional time normalized by ℓ/U_∞, where U_∞ is the freestream velocity; γ is the ratio of specific heats equal to 7/5 for air; and ϕ is the dimensionless perturbation velocity potential. Although a variety of subcases of Eq. (1) exist[4,6] depending upon whether the time behavior of the motion is very slow (quasisteady: ϕ_{xt}, ϕ_{tt} neglected), somewhat more rapid (mildly unsteady: ϕ_{tt} neglected), or very rapid (linear high frequency: $\phi_x\phi_{xx}, \phi_{xt}$ neglected), the authors have considered the more general case, encompassing all frequencies given by Eq. (1).

For the general axisymmetric oscillatory flows considered here, it is convenient to expand the solution into a steady and unsteady component. Thus, set

$$\phi(x,r,\theta,t) = \phi_1(x,r) + \text{R.P.}[\tilde{\phi}(x,r)e^{ikt}] \tag{2}$$

where ϕ_1 is the axisymmetric steady perturbation potential, which satisfies Eq. (1) with the θ and t terms omitted, $\tilde{\phi}$ is the complex amplitude of the oscillatory perturbation velocity potential, k is the reduced frequency defined by $k = \omega\ell/U_\infty$, and R.P. signifies the real part of a complex quantity. Based on the assumption that small-amplitude oscillations are appropriate for flutter and stability analysis, the equation for $\tilde{\phi}$ becomes

$$\tilde{\phi}_{rr} + (1/r)\tilde{\phi}_r = [M_\infty^2 - 1 + M_\infty^2(\gamma+1)\phi_{1x}]\tilde{\phi}_{xx} + [M_\infty^2(\gamma+1)\phi_{1xx} + 2ikM_\infty^2]\tilde{\phi}_x - M_\infty^2\rho^{\cup}\tilde{\phi} \tag{3}$$

which, although linear, nevertheless, remains formidable because of the variable coefficients and mixed elliptic-hyperbolic type.

The boundary condition at the body surface can be decomposed analogously. Upon setting

$$R(x,t) = \epsilon\bar{R}(x) + \text{R.P.}[\delta\tilde{R}(x)e^{ikt}] \tag{4}$$

where $(\bar{R}, \tilde{R})$ are normalized functions describing the steady and oscillatory components of the body ordinates, and (ϵ,δ) are, respectively, the normalized maximum body thickness and the dimensionless amplitude of the unsteady oscillations, one obtains

$$\phi_{1r}(x,R_1) = R_1' + O(\epsilon^3\ell\,n\epsilon) \tag{5a}$$

$$\tilde{\phi}_r(x,R_1) = \delta\left[\tilde{R}' + ik\tilde{R} + \frac{\bar{R}'}{\bar{R}}\tilde{R}\right] + O(\delta\epsilon^2\ell\,n\epsilon\delta^2) \tag{5b}$$

where $R_1 = \epsilon\bar{R}$, and primes indicate differentiation with respect to x. The first two terms on the right-hand side of Eq. (5b) are familiar, since they also appear in the oscillatory thin-wing problem.[5] For the slender body case, however, the third term arises from the imposition of the no-flow boundary condition at the actual oscillating body surface,[7] where a Taylor series expansion about the mean position $r = R_1$ is used to remove the resulting implicit dependence on δ. Finally, the corresponding expressions for the surface pressure coefficients are

$$C_{p_1}(x,R_1) = -2\phi_{1x}(x,R_1) - R_1'^2 \tag{6a}$$

$$\tilde{C}_p(x,R_1) = -2\left[\tilde{\phi}_x(x,R_1) + ik\tilde{\phi}(x,R_1) + \left(R_1'' + \frac{R_1'^2}{R_1}\right)\tilde{R} + R_1'(\tilde{R}' + ik\tilde{R})\right] \tag{6b}$$

Use of the method of matched asymptotic expansions serves to identify the logarithmic behavior of both the steady and unsteady components near the body axis. Consequently, the differential equation and surface boundary condition for the unsteady component can be expressed in the compact form

$$\lambda_1\tilde{\phi}_{xx} + \lambda_2\tilde{\phi}_x + \lambda_3\tilde{\phi} = \tilde{\phi}_{rr} + (1/r)\tilde{\phi}_r \tag{7}$$

$$\lim_{r\to 0}(r\tilde{\phi}_r) = g(x) = \epsilon\delta\bar{R}[\tilde{R}' + ik\tilde{R} + (\bar{R}'/\bar{R})\tilde{R}] \tag{8}$$

where $(\lambda_1, \lambda_2, \lambda_3)$ can be identified from Eq. (3).

Received December 4, 1975; revision received April 5, 1976. This work was supported by the Office of Naval Research under Contract No. N00014-73-C-0379.

Index categories: Nonsteady Aerodynamics, Subsonic and Transonic Flow.

*Senior Research Scientist. Member AIAA.

†Professor, Department of Aeronautics and Astronautics and Mechanical Engineering; also consultant to Nielsen Engineering & Research, Inc. Fellow AIAA.

Three fundamentally different differential equations and solutions occur for $\tilde{\phi}$, depending upon the sign of λ_1; i.e., whether $\lambda_1 < 0$ (subsonic), $\lambda_1 = 0$, (sonic), or $\lambda_1 > 0$ (supersonic). The regions are illustrated in the upper left of Fig. 1 for the forepart of a slender convex body at $M_\infty = 1$. The solution for the sonic region 2 must merge continuously with that for the subsonic region 1 ahead of it and the supersonic region 3 behind it.

The procedure for determining the local linearization solution for the unsteady component $\tilde{\phi}$ requires first that the steady-state solution ϕ_1 be obtained to evaluate the variable coefficients (λ_1, λ_2). Then an approximate solution for $\tilde{\phi}$ is determined by replacing the variable coefficients (λ_1, λ_2) temporarily in Eq. (7) by constants, and solving the simplified equations that result in each of the three regions identified previously. In the original procedure for steady transonic flow, the next step would be to calculate the surface acceleration $d^2\tilde{\phi}(x,R_1)/dx^2$, replace the constants (λ_1, λ_2) by

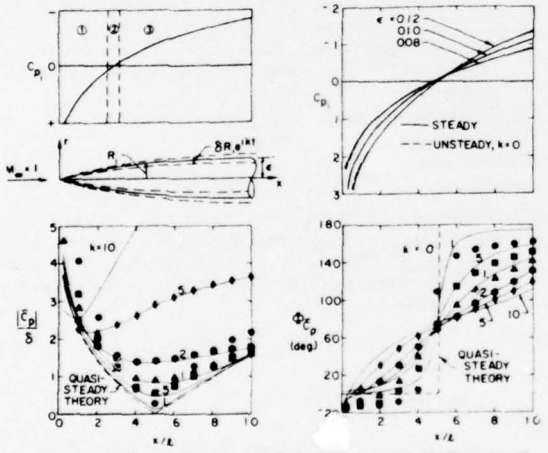

Fig. 1 Unsteady pressure distributions on various parabolic-arc half-bodies undergoing pulsatile surface oscillations; local linearization ——, quasi steady ---, acoustic theory $k=0.01$, ●; $k=0.5$, ■; $k=1.0$, ▲; $k=2.0$, ⬤; $k=5.0$ ◆.

the functions that they original represented, and finally integrate the resultant second-order ordinary differential equation along the body surface to obtain both $d\tilde{\phi}(x,R_1)/dx$ and $\tilde{\phi}(x,R_1)$, to be used in Eq. (6b). In the results reported here, the authors have used a variant of that procedure by calculating $\tilde{\phi}_{,x}(x,R_1)$ and $\tilde{\phi}(x,R_1)$ directly from the simplified equations. Near the body surface, these solutions are

$$\underset{\text{sonic}}{\tilde{\phi}}(x,r) = \frac{1}{2}\left[g(x)\cdot\left\{E_{in}(A_0x) + \ell n\left(\frac{\lambda_2 r^2}{4x}\right) + C\right\} + \int_0^x \frac{g(x)-g(\xi)}{x-\xi}\, e^{-A_0(x-\xi)}\, d\xi\right] \qquad (\lambda_1 \simeq 0) \tag{9}$$

$$\underset{\text{subsonic}}{\tilde{\phi}}(x,r) = \frac{1}{2}\left[g(x)\cdot\left\{E_{in}(A_1x) + E_{in}[-A_2(1-x)] + \ell n\left(\frac{-\lambda_1 r^2}{4x(1-x)}\right)\right\} + \int_0^x \frac{g(x)-g(\xi)}{x-\xi}\, e^{-A_1(x-\xi)}\, d\xi - \int_x^1 \frac{g(\xi)-g(x)}{\xi-x}\, e^{A_2(\xi-x)}\, d\xi\right] \qquad (\lambda_1 < 0) \tag{10}$$

$$\underset{\text{supersonic}}{\tilde{\phi}}(x,r) = \frac{1}{2}\left[g(x)\cdot\left\{E_{in}(A_1x) + E_{in}(A_2x) + \ell n\left(\frac{\lambda_1 r^2}{4x^2}\right)\right\} + \int_0^x \frac{g(x)-g(\xi)}{x-\xi}\left\{e^{-A_1(x-\xi)} + e^{-A_2(x-\xi)}\right\} d\xi\right] \qquad (\lambda_1 > 0) \tag{11}$$

where $E_{in}(Z)$ is the complete exponential function of complex argument Z, [8] C is Euler's constant,

$$A_0 = \lambda_3/\lambda_2, \quad A_1 = [\lambda_2 - (\lambda_2^2 - 4\lambda_1\lambda_3)^{1/2}]/2\lambda_1$$

and

$$A_2 = [\lambda_2 + (\lambda_2^2 - 4\lambda_1\lambda_3)^{1/2}]/2\lambda_1$$

Results determined by employing the solutions given by Eqs. (9-11) in their respective domains, are shown in Fig. 1. Exhibited in the two lower plots are the normalized magnitude and phase (in degrees) of the unsteady surface pressure distributions $\bar{C}_p$ for a parabolic-arc half-body, with $\epsilon = 0.10$ executing pulsatile oscillations of its body surface proportional to the local radius ($\bar{R} = \bar{R}$). In those results, as well as others presented here, the steady solutions required as input to the unsteady calculation were determined by the local linearization method for axisymmetric bodies,[2] which is known to provide good accuracy for the shapes being considered. Also indicated on those plots are the results provided by quasisteady theory and by linear acoustic theory, to which the present results converge for small and large k. The close correspondence between the nonlinear and quasisteady results for $k = 0.1$ implies a substantial nonlinear thickness effect of the steady flow upon the unsteady component at low frequencies, and indicates, furthermore, the quasisteady theory can provide good results in this range. In contrast, the comparisons with acoustic theory indicate large discrepancies for small k, particularly in phase angle, which tend to disappear only when k is approximately 2.

A further evaluation of the low-frequency results predicted by the present method is provided by the plot in the upper right of Fig. 1. The pressure distributions indicated by the unsteady analysis for a basic parabolic-arc half-body, having a maximum thickness $\epsilon = 0.10$, undergoing slow expansion to $\epsilon = 0.12$ and contraction to $\epsilon = 0.08$, are compared with results predicted by the local linearization theory for steady flow past three such bodies. The results are in good agreement, in spite of the linearization of the unsteady component and the substantially different methods of solution.

Figure 2 shows the analogous results for a cone with $\epsilon = 0.10$. Although the analysis derived here applies strictly to smoothly accelerating flows on continuous bodies – a condition severely strained for the flow in the vicinity of the shoulder on a cone – application of the previous techniques is still possible by adopting the strategy of using the unsteady sonic solution predicted by the current method along the entire length of cone. This is plausible, since the subsonic solution, which normally would be joined to the sonic result for points in the region ahead of the shoulder, in fact becomes ill-conditioned; this is because, for a cone, the sonic point is fixed at the end of the body. Again, the quasisteady predictions of the present method shown in the upper right hand

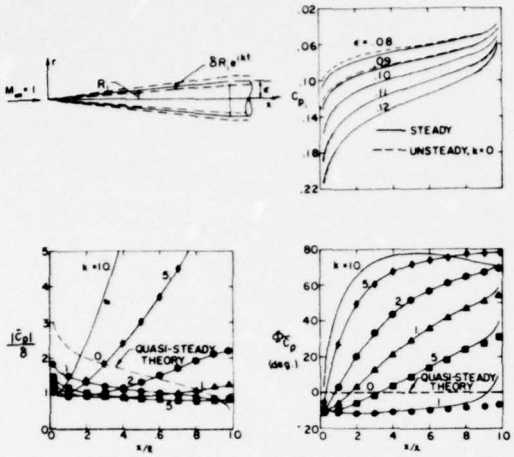

Fig. 2 Unsteady pressure distributions on various cones undergoing pulsatile surface oscillations; local linearization ——, quasi-steady – – –, acoustic theory $k = 0.1$, ●; $k = 0.5$, ■; $k = 1.0$, ▲; $k = 2.0$, ⬤; $k = 5.0$, ◆.

plot of Fig. 2 indicate very good agreement with the steady state results, whereas the comparisons with the acoustic theory results shown in the bottom plots indicate a much more rapid approach to acoustic theory as the frequency increases for a cone, in contrast to a parabolic-arc half body.

References

[1]Spreiter, J.R. and Stahara, S.S., "Unsteady Transonic Aerodynamics – An Aeronautics Challenge," in *Unsteady Aerodynamics, Proceedings of a Symposium held at University of Arizona, March 18-20, 1975*, edited by R. B. Kinney, Vol. II, July 1975, pp. 553-581.

[2]Speiter, J. R. and Alksne, A. Y., "Slender Body Theory Based on Approximate Solution of the Transonic Flow Equation," NASA TR R-2, 1959.

[3]Spreiter, J. R. and Stahara, S.S., "Nonlinear Unsteady Transonic Flow Theory – Local Linearization Solution for Two-Dimensional Flow," *AIAA Journal*, Vol. 13, June 1975, pp. 719-720.

[4]Miles, J. W., *The Potential Theory of Unsteady Supersonic Flow*, Cambridge University Press, New York, 1959.

[5]Landahl, M.T., *Unsteady Transonic Flow*, Pergammon Press, London, 1961.

[6]Landahl, M.T., "Linearized Theory for Unsteady Transonic Flow," in *Symposium Transsonicum*, edited by K. Oswatitisch, Springer-Verlag, Berlin/Gottingen/Heidelberg, 1964, pp. 414-439.

[7]Hoffman, G. H. and Platzer, M. F., "On Supersonic Flow Past Oscillating Bodies of Revolution," *AIAA Journal*, Vol. 4, Feb. 1966, pp. 370-371.

[8]Abramowitz, M. and Stegun, I. A., *Handbook of Mathematical Functions*, National Bureau of Standards, Washington D.C., Aug. 1966, Fifth Printing, p. 228.

Unsteady Local Linearization Solution for Pitching Bodies of Revolution at $M_\infty = 1$: Stability Derivative Analysis

Stephen S. Stahara*
Nielsen Engineering & Research, Inc., Mountain View, Calif.

and

John R. Spreiter†
Stanford University, Stanford, Calif.

An account is provided of recent theoretical results for unsteady inviscid transonic flows about axisymmetric bodies. The unsteady local linearization solution is developed to calculate the unsteady pressure distributions, for sonic or near-sonic freestream flows, on the surface of several slender, pointed, axisymmetric bodies undergoing low-frequency oscillatory pitching motion. Results determined for static and dynamic stability derivatives exhibit good agreement with the limited experimental data available.

Introduction

THE purpose of this paper is to describe a theoretical procedure for determining the unsteady flowfield at freestream Mach numbers at or near one about slender axisymmetric bodies undergoing oscillatory pitching motion. The analysis is based on the small-disturbance theory of inviscid unsteady transonic flow and makes use of the concept of splitting the flow into steady and unsteady components and solving the resultant unsteady potential equation by the local linearization technique. An expansion of the unsteady solution is obtained for low reduced frequencies, for which the nonlinear thickness and Mach number effects of the steady flow are significant, and the Adam-Sears iteration procedure is used to determine the unsteady near-field potential, from which flow properties on the body surface are calculated. The approach generalizes the results of Landahl,[1] Liu,[2] Liu et al.,[3] and Ruo and Liu,[4] both in the sense of encompassing the entire low-frequency range, including $k=0$, and also in eliminating the "parabolic" assumption,[3,4] thereby properly accounting for local regions of subsonic, sonic, and supersonic flow. Applications are made to various parabolic-arc half-bodies and cones at $M_\infty = 1$, and results are presented for unsteady force and moment distributions and static and dynamic stability derivatives. The examples were selected, insofar as possible, to enable comparison with existing data and other theories. We note that alternative approaches, employing the recently developed methods of Isogai[5] and Dowell,[6] that are based on the same general notions of the local linearization method are also possible and would provide an interesting further comparison of these different procedures.

Analysis

Basic Equations

The analysis is developed in terms of a body-fixed cylindrical coordinate system centered at the nose with the x axis directed rearward and aligned with the longitudinal axis of the body, and the $\theta = 0$ deg axis directed to the right, facing forward. A slender, pointed body of revolution immersed in a zero angle-of-attack steady flow is assumed to undergo small-amplitude harmonic pitching oscillations about a point located on the body axis at $x=a$. With the fundamental assumption that the body is sufficiently smooth and slender so that the inviscid small disturbance theory applies, a perturbation velocity potential ϕ may be defined according to[7]

$$\Phi(x,r,\theta,t) = U_\infty [\,(x-a)\ \cos\delta + r\ \sin\theta\ \sin\delta + \phi(x,r,\theta,t)\,] \tag{1}$$

where U_∞ represents the freestream velocity. The angular displacement $\delta(t)$ is given by

$$\delta(t) = RP[\delta_0 e^{ikt}] \tag{2}$$

where δ_0 is the maximum displacement, RP signifies the real part of a complex quantity, k is the reduced frequency defined by $k = \omega\ell/U_\infty$, and ϕ satisfies

$$(1-M_\infty^2)\phi_{xx} + \phi_{rr} + \frac{1}{r}\phi_r + \frac{1}{r^2}\phi_{\theta\theta} = M_\infty^2(\gamma+1)\phi_x\phi_{xx} + M_\infty^2\phi_{rr} + 2M_\infty^2\phi_{xr} \tag{3}$$

In Eq. (3), M_∞ is the freestream Mach number; (x,r,θ) are nondimensional body-fixed cylindrical coordinates with (x,r) normalized by body length ℓ; t is nondimensional time normalized by ℓ/U_∞; and γ is the ratio of specific heats equal to 7/5 for air.

For the oscillatory flows considered here, it is convenient to expand the solution into a steady and unsteady component. Thus, we set

$$\phi(x,r,\theta,t) = \phi_1(x,r) + RP[\tilde{\phi}(x,r)\ \sin\theta e^{ikt}] \tag{4}$$

where ϕ_1 is the axisymmetric steady perturbation potential, which satisfies Eq. (3) with the (θ,t) terms omitted, and $\tilde{\phi}$ is the complex amplitude of the oscillatory perturbation velocity potential. On the assumption of small amplitude oscillations appropriate for flutter and stability analysis, the equation for $\tilde{\phi}$ becomes

$$\tilde{\phi}_{rr} + \frac{1}{r}\tilde{\phi}_r - \frac{1}{r^2}\tilde{\phi} = [M_\infty^2 - 1 + M_\infty^2(\gamma+1)\phi_{1x}]\tilde{\phi}_{xx} + M_\infty^2(\gamma+1)\phi_{1xx} + 2ikM_\infty^2]\tilde{\phi}_x - M_\infty^2 k^2\tilde{\phi} \tag{5}$$

Received Feb. 23, 1976; revision received June 23, 1976. This work was supported by the Office of Naval Research under Contract N00014-73-C-0379.

Index categories: Nonsteady Aerodynamics, Subsonic and Transonic Flow.

*Senior Research Scientist. Member AIAA.

†Professor, Departments of Aeronautics and Astronautics and of Mechanical Engineering. Consultant to Nielsen Engineering & Research, Inc. Fellow AIAA.

which, although being linear, is formidable to solve because of the variable coefficients and mixed elliptic-hyperbolic type.

The boundary condition of flow tangency at the body surface can be decomposed analogously. In the body-fixed coordinate system, these conditions are[7]

$$\phi_{1_r}(x,R) = R' + 0(\epsilon^3 \ln\epsilon) \tag{6a}$$

$$\tilde{\phi}_r(x,R) = \delta_0[1 + k(x-a)] + R'\tilde{\phi}_x(x,R) - ik\delta_0 RR' + 0(\delta_0\epsilon^4 \ln\epsilon, \delta_0^2) \tag{6b}$$

where $R = \epsilon\bar{R}(x)$ describes the body ordinates. Here, ϵ is the normalized maximum body thickness, and $\bar{R}$ is a function of order one. At infinity, the perturbation potentials are required to vanish in an appropriate manner. Since attention will be confined to flows with $M_\infty \approx 1$ having all shock waves downstream of the region for which results will be calculated, we will not require the corresponding relation for conditions on the two sides of a shock wave. The preceding equations provide, therefore, the fundamental relations for the analysis to follow.

Local Linearization Solution

The differential equation (5) for the unsteady component can be expressed in the compact form

$$\lambda_1\tilde{\phi}_{xx} + \lambda_2\tilde{\phi}_x + \lambda_3\tilde{\phi} = \tilde{\phi}_{rr} + \frac{1}{r}\tilde{\phi}_r - \frac{1}{r^2}\tilde{\phi} \tag{7}$$

where

$$\lambda_1 = M_\infty^2 - 1 + M_\infty^2(\gamma+1)\phi_{1x}, \qquad \lambda_2 = M_\infty^2(\gamma+1)\phi_{1xx} + i2kM_\infty^2, \qquad \lambda_3 = -k^2M_\infty^2$$

Three fundamentally different differential equations and solutions occur for $\tilde{\phi}$ depending upon whether the coefficient λ_1, which corresponds in the small-disturbance approximation to $M_{\text{local}}^2 - 1$, is negative, near zero, or positive.[8] The zone of influence of each solution is different for each case, as is appropriate since they correspond to local regions of subsonic, sonic, or supersonic flow. Each solution then forms the basis of the ensuing analysis in its appropriate region, with the requirement that each partial solution is required to merge continuously with that for the adjacent region. The local linearization method proceeds by replacing temporarily the variable coefficients (λ_1,λ_2) in Eq. (7) by constants and solving the simplified equations that result in each of the three regions discussed above. Next, the quantities $\tilde{\phi}_x(x,R)$ and $\tilde{\phi}(x,R)$, which are required for evaluating surface properties of the flow, such as the unsteady pressure coefficient, are determined by first obtaining them from the simplified equations, then replacing the constants (λ_1,λ_2) by the functions they originally represented, and finally evaluating the resulting expressions at points along the body.

The three starting solutions for $\tilde{\phi}$ are given by

$$\tilde{\phi}_{\text{sonic}}(x,r) = \frac{1}{2}\frac{\partial}{\partial r}\int_0^x \frac{g(\xi)\ \exp\left[-A_0(x-\xi) - \dfrac{\lambda_2 r^2}{4(x-\xi)}\right]}{x-\xi}\,d\xi \quad (\lambda_1 \simeq 0) \tag{8}$$

$$\tilde{\phi}_{\text{subsonic}}(x,r) = \frac{1}{2}\frac{\partial}{\partial r}\int_0^x \frac{g(\xi)\ \exp[-A_1(x-\xi) + A_2[(x-\xi)^2 + (-\lambda_1)r^2]^{1/2}]}{[x-\xi)^2 + (-\lambda_1)r^2]^{1/2}}\,d\xi \quad (\lambda_1 < 0) \tag{9}$$

$$\tilde{\phi}_{\text{supersonic}}(x,r) = \frac{1}{2}\frac{\partial}{\partial r}\int_0^{x-\sqrt{\lambda_1}r} \frac{g(\xi)\exp[-A_1(x-\xi)]\cosh[A_2[A_2[(x-\xi)^2 - \lambda_1 r^2]^{1/2}]}{[(x-\xi^2 - \lambda_1 r^2]^{1/2}}\,d\xi \quad (\lambda_1 > 0) \tag{10}$$

where $g(x)$ is the doublet strength to be determined later from the boundary condition,

$$A_0 = \lambda_3/\lambda_2, \quad A_1 = \lambda_2/2\lambda_1, \quad \text{and} \quad A_2 = \sqrt{\lambda_2^2 - 4\lambda_1\lambda_3}\,/2\lambda_1$$

In determining the local linearization solution, the forms of these solutions in the near field are required. These could be obtained by expanding the above solutions directly for small r; however, a more convenient method is to Fourier transform the basic equation (7) for the three different regions with respect to x, solve the transformed equations, expand the Kernel functions in the transformed solutions for small r, and then transform the simplified results back to the physical plane. Use of either technique leads, after much manipulation, to the following forms:

$$\tilde{\phi}_{\text{sonic}}(x,r) = -\left[\frac{g(x)}{r} + \frac{r}{4}\left\{\Lambda(x)\left[E_{in}(A_0x) + \ln\left(\frac{\lambda_2 r^2}{4x}\right) + C - 1\right]\right.\right.$$
$$\left.\left. + \int_0^x \frac{\Lambda(x) - \Lambda(\xi)}{x-\xi}e^{-A_0(x-\xi)}\,d\xi - \lambda_2 g(0)\frac{e^{-A_0x}}{x}\right\}\right] + 0(r^3\ln r) \quad (\lambda_1 \simeq 0) \tag{11}$$

$$\tilde{\phi}_{\text{subsonic}}(x,r) = -\left[\frac{g(x)}{r} + \frac{r}{4}\left\{\Lambda(x)\left\{E_{in}(A_3x) + E_{in}[-A_4(1-x)]\right\} + \ln\left[\frac{-\lambda_1 r^2}{4x(1-x)}\right] - 1\right\}\right.$$
$$+ \int_0^x \frac{\Lambda(x) - \Lambda(\xi)}{x-\xi}e^{-A_3(x-\xi)}d\xi - \int_x^1 \frac{\Lambda(\xi) - \Lambda(x)}{\xi - x}e^{A_4(\xi-x)}d\xi$$
$$\left. + \left\{\left[\lambda_1\left(\frac{1}{x} + A_3\right) - \lambda_2\right]g(o) - \lambda_1 g'(o)\right\}\frac{e^{-A_3x}}{x} + \left\{\left[\lambda_1\left(\frac{1}{1-x} - A_4\right) + \lambda_2\right]g(1) + \lambda_1 g'(o)\right\}\frac{e^{A_4(1-x)}}{1-x}\right\}\right] + 0(r^3\ln r) \quad (\lambda_1 < o) \tag{12}$$

$$\tilde{\phi}(x,r)_{\text{supersonic}} = -\left[\frac{g(x)}{x}\right]^{\sim} + \frac{r}{4}\left\{\Lambda(x)\left[E_{in}(A_3 x) + E_{in}(A_4) + \ln\left(\frac{\lambda_1 r^2}{4x^2}\right) - 1\right] + \int_0^x \frac{\Lambda(x)-\Lambda(\xi)}{x-\xi}\left[e^{-A_3(x-\xi)} + e^{-A_4(x-\xi)}\right]d\xi\right.$$

$$\left. + \left\{\left[\lambda_1\left(\frac{1}{x}+A_3\right)-\lambda_2\right]e^{-A_3 x} + \left[\lambda_1\left(\frac{1}{x}+A_4\right)-\lambda_2\right]e^{-A_4 x}\right\}\frac{g(o)}{x} - \lambda_1\left(e^{-A_3 x}+e^{-A_4 x}\right)\frac{g'(o)}{x}\right\}\right] + O(r^3 \ln r) \quad (\lambda_1 > 0) \tag{13}$$

where

$$\Lambda(x) \equiv \lambda_1 g''(x) + \lambda_2 g'(x) + \lambda_3 g(x)$$

$E_{in}(Z)$ is the complete exponential function of complex argument Z[9], $C = 0.577216$ is Euler's constant,

$$A_3 = (\lambda_2 - \sqrt{\lambda_2^2 - 4\lambda_1\lambda_3})/2\lambda_1,$$

and

$$A_4 = (\lambda_2 + \sqrt{\lambda_2^2 - 4\lambda_1\lambda_3})/2\lambda_1$$

Low Frequency Solution

Of primary importance in this investigation are low frequency oscillations, that is, $k = 0(\epsilon^2 \ln\epsilon)$, where the nonlinear thickness and Mach number effects of the steady flow strongly influence the unsteady flow. For this frequency regime, it is convenient to decompose the unsteady component in the following manner

$$\tilde{\phi}(x,r)e^{ikt} = \delta\tilde{\phi}^{i}(x,r) + \delta\tilde{\phi}^{o}(x,r) \tag{14}$$

where $\delta = ik\delta$ and the superscripts (i,o) denote, respectively, the in-phase and out-of-phase unsteady components.

What remains now is to obtain to appropriate order the doublet distribution $g(x)$ appearing in Eqs. (11-13). An effective means employed in similar investigations[1-4] is to make use of the Adam-Sears technique. If we represent the doublet distribution and potential by

$$g(x) = g_1(x) + g_2(x) \tag{15}$$

$$\tilde{\phi}^{i,o}(x,r) = \tilde{\phi}_1^{i,o}(x,r) + \tilde{\phi}_2^{i,o}(x,r) \tag{16}$$

where $g_1(x)$ and $\tilde{\phi}_1^{i,o}(x,r)$ represent the first-order effects, whereas $g_2(x)$ and $\tilde{\phi}_2^{i,o}(x,r)$ are of a higher unspecified order, application of the surface boundary condition equation (6) serves to determine the distributions (g_1, g_2) explicitly, and, from these, the solution for the near-field potential follows directly. The result of these operations-after taking into account that $\lambda_1 = 0(\epsilon^2 \ln\epsilon), \lambda_2 = 0(\epsilon^2 \ln\epsilon) + 0(k), \lambda_3 = 0(k^2), \delta = ik\delta$, ignoring $0(k^2)$ terms, and retaining terms in the near-field potentials to $0(\epsilon^4, \epsilon^2 \ln\epsilon)$ as is consistent with the boundary condition equation (6) – is that $g_1 = 0(\epsilon^2), \tilde{\phi}_1^{i,o} = 0(\epsilon^2/r)$ represent the slender-body doublet, whereas $g_2 = 0(\epsilon^4, \epsilon^4 \ln\epsilon), \tilde{\phi}_2^{i,o} = 0(\epsilon^4/r, \epsilon^2 r \ln r, \epsilon^2 r)$ represent the second-order correction due to body thickness, reduced frequency, and Mach number. Specifically, we find that

$$\begin{Bmatrix} \tilde{\phi}^{i} \\ \tilde{\phi}^{o} \end{Bmatrix} = \begin{Bmatrix} \tilde{\phi}_1^{i}(x,r) \\ \tilde{\phi}_1^{o}(x,r) \end{Bmatrix} + \begin{Bmatrix} \tilde{\phi}_2^{i}(x,r) \\ \tilde{\phi}_2^{o}(x,r) \end{Bmatrix} + O(\epsilon^4 \ln\epsilon) \text{ for } r = O(\epsilon) \tag{17}$$

where

$$\begin{Bmatrix} \tilde{\phi}_1^{i} \\ \tilde{\phi}_1^{o} \end{Bmatrix} = \begin{Bmatrix} 1 \\ x-a \end{Bmatrix} \frac{Q(x)}{\pi r} \tag{18}$$

and

$$\tilde{\phi}_2^{i} = -\frac{Q'^2(x)}{4\pi^2 r} \tag{19}$$

$$\tilde{\phi}_{2\,\text{sonic}}^{o}(x,r) = \frac{1}{4\pi}\left[\frac{Q(x)}{\pi r} + r\right]\left[2M_\infty^2\left\{Q'(x)\left[\ln\left(\frac{|\lambda_2|}{4x}\right) + C + 1 + \frac{\tan^{-1}\left(\frac{2kM_\infty^2}{\lambda_{2RP}}\right)}{\left(\frac{2kM_\infty^2}{\lambda_{2RP}}\right)}\right] + \int_0^x \frac{Q'(x)-Q'(\xi)}{x-\xi}d\xi\right\}\right] + \Delta\tilde{\phi}(x,r) \tag{20}$$

$$\tilde{\phi}_{2\,\text{subsonic}}^{o}(x,r) = \frac{1}{4\pi}\left[\frac{Q(x)}{\pi r} + r\right]\left[2M_\infty^2\left(Q'(x)\left\{E_{in}\left[-\frac{\lambda_2}{\lambda_1}(1-x)\right]_{RP} + \ln\left[-\frac{\lambda_1}{4x(1-x)}\right] + 1\right\} + \int_0^x \frac{Q'(x)-Q'(\xi)}{x-\xi}d\xi\right.\right.$$

$$\left. - \int_0^1 \frac{Q'(\xi)-Q'(x)}{\xi-x}\left[e^{(\lambda_2/\lambda_1)(\xi-x)}\right]_{RP}d\xi\right) + \left[\lambda_1 Q''(x) + \lambda_{2RP}Q'(x)\right]\left\{\frac{E_{in}\left[-\frac{\lambda_2}{\lambda_1}(1-x)\right]}{k}\right\}_{IP}$$

$$\left. + \int_x^1 \frac{\lambda_1[Q''(\xi)-Q''(x)] + \lambda_{2RP}[Q'(\xi)-Q'(x)]}{\xi-x}\left[\frac{e^{(\lambda_2/\lambda_1)(\xi-x)}}{k}\right]_{IP}d\xi + \frac{\lambda_1}{(1-x)}\left[\frac{Q(x)}{1-x} + Q'(1)\right]\left[\frac{e^{(\lambda_2/\lambda_1)(1-x)}}{k}\right]_{IP}\right] + \Delta\tilde{\phi}(x,r) \tag{21}$$

$$\tilde{\phi}_2^o(x,r)_{\text{supersonic}} = \frac{1}{4\pi}\left[\frac{Q(x)}{\pi r}+r\right]\left[2M_\infty^2\left\{Q'(x)\left[E_{in}\left(\frac{\lambda_2}{\lambda_1}x\right)_{RP}+\ln\left(\frac{\lambda_1}{4x^2}\right)+1\right]\right.\right.$$

$$+\int_0^x \frac{Q'(x)-Q'(\xi)}{x-\xi}\left[1+e^{-(\lambda_2/\lambda_1)(x-\xi)^2}\right]_{RP}d\xi\Big\}+\Big[\lambda_1 Q''(x)$$

$$\left.\left.+\lambda_{2_{RP}}Q'(x)\right]\left[\frac{E_{in}\left(\frac{\lambda_2}{\lambda_1}x\right)}{k}\right]_{IP}+\int_0^x\frac{\lambda_1[Q''(x)-Q''(\xi)]+\lambda_{2RP}[Q'(x)-Q'(\xi)]}{x-\xi}d\xi\right]+\Delta\tilde{\phi}(x,r) \tag{22}$$

where

$$\Delta\tilde{\phi}(x,r) = -\frac{(x-a)Q'^2(x)}{4\pi^2 r}+\frac{M_\infty^2 Q'(x)}{2\pi}\left[\frac{Q(x)}{\pi r}\ln\frac{Q(x)}{\pi}+r\ln r^2\right] \tag{23}$$

In Eqs. (20) to (22), the coefficients (λ_1,λ_2) are evaluated on the body surface $r=R$ and, consequently, are functions of x only,

$$\lambda_{2_{RP}} = RP(\lambda_2) = M_\infty^2(\gamma+1)\phi_{1_{xx}}(x,R) \tag{24}$$

$Q(x)$ represents the body area distribution, and is given by $Q(x)=\pi R^2(x)$ and IP signifies the imaginary part of a complex quantity. Also, implicit in those equations are the appropriate limiting forms as $k\to 0$. For example,

$$\lim_{k\to 0}\left[\frac{\tan^{-1}\left(\frac{2kM_\infty^2}{\lambda_{2RP}}\right)}{\left(\frac{2kM_\infty^2}{\lambda_{2RP}}\right)}\right]=1+0(k^2) \tag{25}$$

$$\lim_{k\to 0}\left\{\frac{E_{in}\left[-\frac{\lambda_2}{\lambda_1}(1-x)\right]}{k}\right\}_{IP}=\frac{2M_\infty^2}{\lambda_{2_{RP}}}\left[1-e^{(\lambda_{2RP})\lambda_1(1-x)}\right]+0(k^2) \tag{26}$$

We note that the present sonic region results are in agreement with the low-frequency parabolic-method results of Refs. 3 and 4 when several higher order terms (in ϵ) inconsistently included in those results are omitted. With $\tilde{\phi}(x,r)$ known, the surface pressure coefficient can be determined for low-frequency, small-amplitude oscillations from the result[7] that

$$C_p(x,R,\theta,t) = C_{p_1}(x,R)+[\delta\tilde{C}_p^i(x,R)+\delta\tilde{C}_p^o(x,R)]\sin\theta \tag{27}$$

where the steady pressure coefficient is given by

$$C_{p_1}(x,R) = -2\phi_{1_x}(x,R)-R'^2 \tag{28}$$

while the in-phase and out-of-phase unsteady pressures are

$$\tilde{C}_p^i(x,R) = -2\tilde{\phi}_{1_x}^i(x,R)+2\left\{[(1-M_\infty^2)\phi_{1_x}(x,R)-\left(1-\frac{M_\infty^2}{2}\right)R'^2]\tilde{\phi}_{1_x}^i(x,R)-\tilde{\phi}_{2_x}^i(x,R)\right\}=\tilde{C}_{p_1}^i(x,R)+\tilde{C}_{p_2}^i(x,R) \tag{29}$$

$$\tilde{C}_p^o(x,R) = -2[\tilde{\phi}_{1_x}^o(x,R)+\tilde{\phi}_1^i(x,R)]+2\Big\{\Big[(1-M_\infty^2)\phi_{1_x}(x,R)-\left(1-\frac{M_\infty^2}{2}\right)R'^2\Big]\tilde{\phi}_{1_x}^o(x,R)$$

$$+[M_\infty^2\phi_{1_x}(x,R)+\frac{1}{2}M_\infty^2R'^2]\tilde{\phi}_1^i(x,R)+R\phi_{1_x}(x,R)+RR'^2-\tilde{\phi}_{2_x}^o(x,R)-\tilde{\phi}_2^i(x,R)\Big\}=\tilde{C}_{p_1}^o(x,R)+\tilde{C}_{p_2}^o(x,R) \tag{30}$$

where $(\tilde{C}_{p_1}^{i,o}\ \tilde{C}_{p_2}^{i,o}$ represent, respectively, the first- and second- order unsteady pressure coefficients. From these, the flutter and stability derivatives can be calculated directly using

$$\begin{Bmatrix}C_{M_\delta}\\C_{M_{\dot\delta}}\end{Bmatrix}_{1,2}=-\frac{1}{\epsilon^2}\int_0^1\left[(x-a)\begin{Bmatrix}\tilde{C}_p^i(x,R)\\\tilde{C}_p^o(x,R)\end{Bmatrix}_{1,2}+R(x)R'(x)\begin{Bmatrix}\tilde{C}_p^i(x,R)\\\tilde{C}_p^o(x,R)\end{Bmatrix}_1\right]dx$$

$$\begin{Bmatrix}C_{N_\delta}\\C_{N_{\dot\delta}}\end{Bmatrix}_{1,2}=-\frac{1}{\epsilon^2}\int_0^1 R(x)\begin{Bmatrix}C_p^i(x,R)\\C_p^o(x,R)\end{Bmatrix}_{1,2}dx \tag{31}$$

where again the subscripts (1,2) serve to identify the first-and second-order components of the various derivatives.

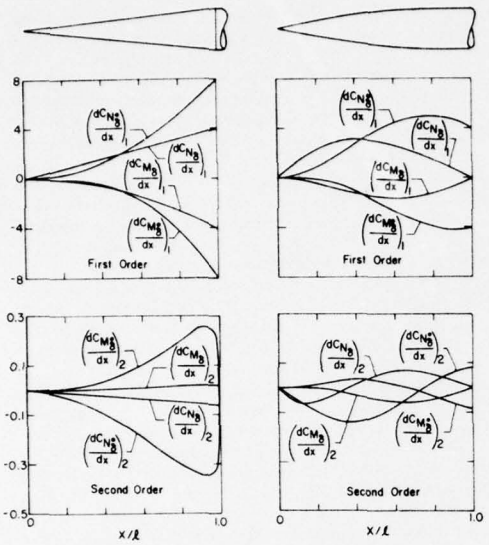

Fig. 1 Distributions of first- and second-order flutter derivatives for a cone and a parabolic half-body with $\epsilon = 0.1$ oscillating in pitch about $x = 0$ at $M_\infty = 1$.

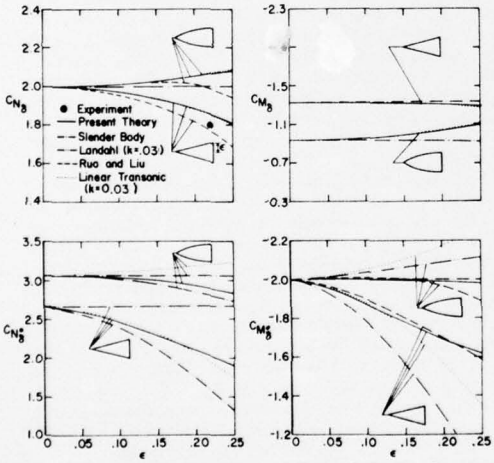

Fig. 2 Thickness ratio dependence of flutter derivatives for cones and parabolic half-bodies oscillating in pitch about $a = 0$ at $M_\infty = 1$.

Results

In order to demonstrate the effects of thickness ratio, reduced frequency, pitch axis location, and body geometry on the unsteady motion, the results of the previous analysis were applied to various finite-length circular cones and parabolic-arc half-bodies described, respectively, by

$$\left.\begin{aligned} R(x) &= \epsilon x \\ R(x) &= \epsilon(2x - x^2) \end{aligned}\right\} \quad 0 \le x \le l \tag{32}$$

Static and dynamic flutter derivations, as well as their variation along the body surface, were calculated for $M_\infty = 1$. In the results presented, the steady-state solutions required as input to the unsteady calculations were determined by the

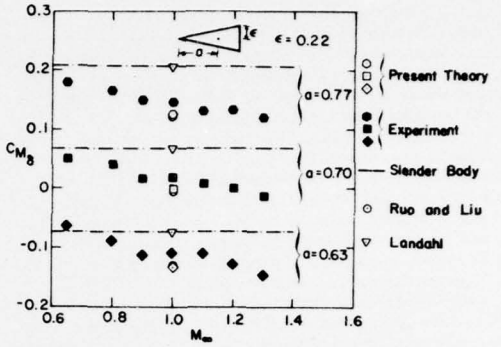

Fig. 3 Pitch moment flutter derivative for a 12.5 deg half-angle cone at $M_\infty = 1$.

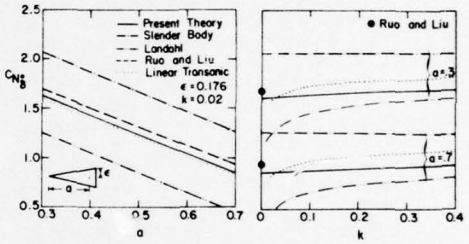

Fig. 4 Pitch axis and frequency dependence of damping-in-pitch normal-force coefficient of a 10 deg half-angle cone at $M_\infty = 1$.

local linearization method,[10] which is known to provide results of good accuracy for the shapes considered here.

Figure 1 exhibits in the left-hand plots the distributions of the first- and second-order static $(dC_{N_\delta}/dx, dC_{M_\delta}/dx)_{1,2}$ and dynamic $(dC_{N_{\dot\delta}}/dx, dC_{M_{\dot\delta}}/dx)_{1,2}$ flutter derivatives for a cone having a maximum thickness $\epsilon = 0.1$ undergoing slow oscillations in pitch about its nose at $M_\infty = 1$. We note in particular the rapid variation of the second-order dynamic derivatives $(dC_{N_{\dot\delta}}/dx, dC_{M_{\dot\delta}}/dx)_2$ in the vicinity of the shoulder, a result of the logarithmic behavior of the steady-state solution[10] in that region. Analogous results for a parabolic-arc half-body are given in the right-hand plots. No large gradients are present in those results, but, as expected, a smooth variation is indicated of the various derivatives along the entire length of the body. The parabolic-arc results for the second-order distributions of normal force $(dC_{N_\delta}/dx)_2$ and damping-in-pitch normal force $(dC_{N_{\dot\delta}}/dx)_2$ presented here agree in trend but differ somewhat in magnitude with those determined by the "parabolic" method.[3] Those results would correspond to using the sonic results of the present method over the entire body with the additional provision that the surface acceleration [see Eq. (24)] is held constant at some representative value.[10]

Figure 2 provides the thickness-ratio dependence of the present theory for the static $(C_{N_\delta}, C_{M_\delta})$ and dynamic $(C_{N_{\dot\delta}}, C_{M_{\dot\delta}})$ flutter derivatives for both cones and parabolic-arc half-bodies oscillating in pitch about the nose at the reduced frequency $k = 0.03$ and $M_\infty = 1$. Also shown for comparison are various available theoretical and experimental results. These include the results of Landahl,[1] the linear transonic method of Liu,[2] the "parabolic" method of Ruo and Liu,[4] and the results of slender body theory, together with experimental data of Wehrend[11] for the normal-force coefficient slope C_{N_δ} of a 12.5 deg half-angle cone with a flat base. Considering first the static derivative comparisons shown in the two upper plots, we note that Landahl's results for

$(C_{N_\delta}, C_{M_\delta})$ are only first order in thickness ratio and consequently identical to slender-body theory. The linear transonic theory results of Liu[2] for $(C_{N_\delta}, C_{M_\delta})$ are identical to the present results for zero frequency; however, those results contain in addition terms linear in k that, for the frequency regime considered here, are of higher order and do not enter into the present results. Comparison with results of the "parabolic" method of Ruo and Liu[4] for C_{N_δ} indicate considerable discrepancy from the present results as the thickness ratio increases and presumably is due to the inconsistent inclusion of higher order terms $0(\epsilon^6 \ln\epsilon/r, r\epsilon^4 \ln\epsilon)$ in that calculation. For the dynamic derivative comparisons shown in the two lower plots, large discrepancies and different trends exist among the various theories. Because Landahl's results are based upon a lower order surface boundary condition, as well as a less accurate force and moment determination, those results can be expected to deviate from the more exact treatment used in the present analysis and those of Liu[2] and Ruo and Liu[4] as the thickness ratio increases. With regard to the comparisons of the linear transonic theory results of Liu,[2] we note that, for the parabolic-arc half-bodies, the failure of that theory to include the effect of the nonlinear steady flow on the unsteady problem is sufficient to change the entire trend of the dependence of the dynamic stability derivatives on thickness ratio. This provides yet another example of both the sensitivity and dependence of the unsteady motion on the nonlinear steady flow at transonic speeds and points out the necessity of including this effect.

A final comparison of static derivative results of the present method with experiment is provided in Fig. 3. Here, the data obtained by Wehrend[11] for the slope of the pitching moment coefficient C_{M_δ} is shown for a 12.5 deg half-angle cone for three different pitch axes locations at, respectively, 63 percent, 70 percent, and 77 percent of the body length from the nose and for freestream Mach numbers from 0.65 to 1.30. Also provided are the theoretical results of the present method for $M_\infty = 1$, as well as those of Landahl,[1] Ruo and Liu,[4] and slender-body theory. We note again that the linear transonic theory results of Liu[2] for the static derivatives are essentially identical to the present theory and have been omitted for clarity of presentation. Good agreement of the present results is noted with both experiment and the "parabolic" results of Ruo and Liu.[4]

Figure 4 displays the pitch axis and frequency dependence predicted by the present method for the damping-in-pitch normal-force coefficient C_{N_δ} of a 10 deg half-angle cone oscillating in pitch at $M_\infty = 1$. Shown for comparison are the results of Landahl,[1] the linear transonic method of Liu,[2] the "parabolic" method used by Ruo and Liu,[4] and slender-body theory. Significant differences among the various results are observed. Moreover, the well-known logarithmic singularity predicted both by Landahl's method[1] and linear transonic theory[2] as the reduced frequency $k \to 0$ is quite evident, and is in distinct contrast to the smooth variation with k of the present theory. Moreover, we note that the results of Ruo and Liu,[4] which are valid only for very low (quasisteady) frequencies and which do not contain an explicit dependence on k, compare favorably with the present theory near $k = 0$.

A further comparison of the results for the damping-in-pitch normal-force coefficient is provided in Fig. 5, which displays the influence of body shape on both the pitch axis and frequency dependence of C_{N_δ}. Here, various theoretical results for a cone are shown in the two upper plots and are contrasted in the lower plots with the results for a parabolic-arc half-body having the same normalized maximum thickness $\epsilon = 0.10$. Greater disagreement exists among the results of the various theories for the conical rather than the parabolic-arc shape, a fact already observed in the thickness-ratio comparisons of $(C_{N_\delta}, C_{M_\delta})$ shown in Fig. 2. This is almost certainly a result of the particular behavior of the flow in the vicinity of the shoulder of conical bodies, where rapid variations in flow properties occur – an effect altogether absent in the smoothly continuous flow about parabolic-arc half-bodies.

Results analogous to those given in Fig. 4 and 5 are presented in Figs. 6 and 7 for the damping-in-pitch moment coefficient C_{M_δ}. In Fig. 6, results for the damping-in-pitch moment coefficient C_{M_δ} of a 12.5 deg half-angle cone at $M_\infty = 1$ are exhibited. In addition to the theoretical results indicated, experimental data of Wehrend[11] for pitch axes locations $a = 0.63$, 0.70, and 0.77 are also included in the plot on the left. We note that although the present theory provides results somewhat closer to the data than the other methods, none of the theoretical results can be considered to be in acceptable agreement with the data. A feature that introduces additional uncertainty into these comparisons is that the actual flow past a cone with flat base will contain a free streamline emanating from the shoulder whose predicted location is beyond the scope of an inviscid theory. Whereas the direction of that streamline will undoubtedly be close to freestream and its influence restricted essentially to the vicinity of the cone shoulder, inviscid theory predicts that the surface pressures will be unaffected by this feature of the flow, as the influence of its effect is limited to regions of the flow field downstream of the limiting characteristic emanating from the cone shoulder. Discrepancies associated with this effect, together with other uncertainties related to the dynamic testing,[11] are difficult to assess further without additional experiment and analysis. With regard to Fig. 6, we observe again the differences between the various methods, particularly as shown in the plot on the right at low frequen-

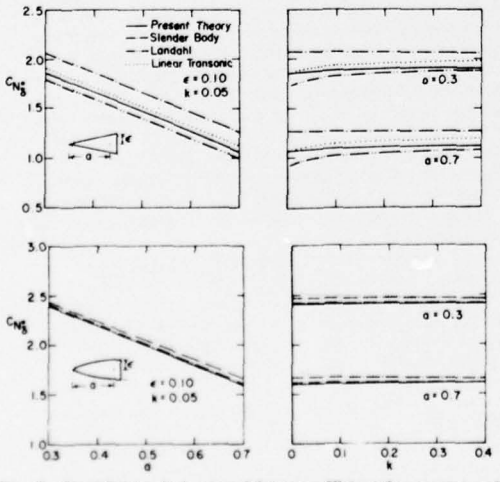

Fig. 5 Damping-in-pitch normal-force coefficient for a cone and parabolic half-body with $\epsilon = 0.1$ at $M_\infty = 1$.

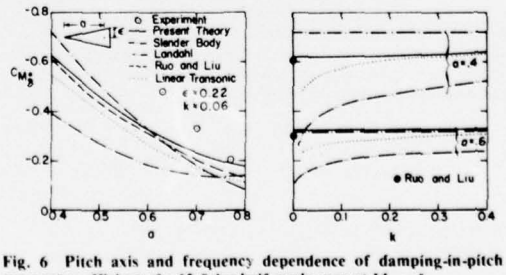

Fig. 6 Pitch axis and frequency dependence of damping-in-pitch moment coefficient of a 12.5 deg half-angle cone at $M_\infty = 1$.

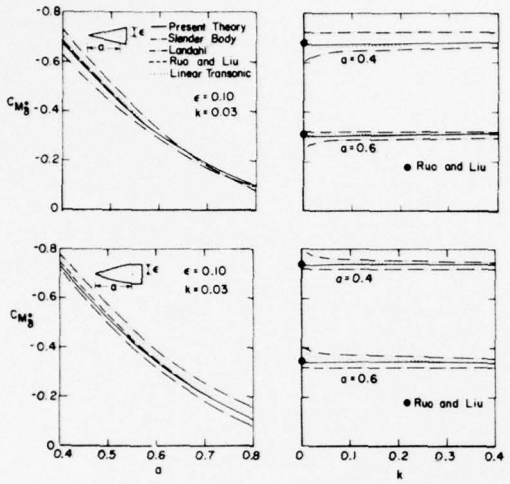

Fig. 7 Damping-in-pitch moment coefficient for a cone and parabolic half-body with $\epsilon = 0.1$ at $M_\infty = 1$.

cies and note the smooth variation with frequency of the present results.

Finally, an assessment of the effect of body shape on C_{M_δ} is provided in Fig. 7, which compares the pitch axis and frequency dependence for a cone and parabolic half-body with $\epsilon = 0.10$ at $M_\infty = 1$. We note in these results the relative closeness of the different methods for both the cone and parabolic half-body.

Concluding Remarks

In this paper, we have given an account of a theoretical study to calculate unsteady surface pressure distributions and stability derivatives for slender, pointed, axisymmetric bodies undergoing low-frequency pitching oscillations in a flow with sonic or near-sonic freestream velocity. The results are shown to be in good agreement with the limited experimental data available for comparison. Additional testing is needed, particularly for the dynamic derivatives, to provide a definitive evaluation of the theoretical predictions.

Finally, we note that the local linearization procedures by which the solutions have been obtained are not restricted to the particular examples displayed in this paper but possess greater generality. The present results, in fact, provide yet another application of the method demonstrating the remarkable ability of the technique to obtain both an accurate and economical approximation to a difficult nonlinear problem.

References

[1] Landahl, M. T., "Forces and Moments on Oscillating Slender Wing-Body Combinations at Sonic Speed," Air Force Office of Scientific Research, Washington, D.C., OSR TN No. 56-109, 1956.

[2] Liu, D. D., "Quasi-Slender Body Theory for Unsteady Linearized Transonic Flow Past Pointed Bodies of Revolution," LSMC/HREC A79 1435, 1968.

[3] Liu, D. D., Platzer, M. F., and Ruo, S. Y., "On the Calculation of Static and Dynamic Stability Derivatives for Bodies of Revolution at Subsonic and Transonic Speeds," AIAA Paper 70-190, New York, 1970.

[4] Ruo, S. Y. and Liu, D. D., "Calculation of Stability Derivatives for Slowly Oscillating Bodies of Revolution at Mach 1.0," LSMC/HREC DI 62375, 1971.

[5] Isogai, K., "A Method for Predicting Unsteady Aerodynamic Forces on Oscillating Wings with Thickness in Transonic Flow Near Mach 1," National Aerospace Lab., Tokyo, Japan, TN NAL-TR-368T, June 1974.

[6] Dowell, E. H., "A Simplified Theory for Oscillating Airfoils in Transonic Flow," *Unsteady Aerodynamics – Proceedings of a Symposium*, University of Arizona, Vol. 2, 1975, pp. 655-680.

[7] Platzer, M. F. and Hoffman, G. H., "Quasi-Slender Body Theory for Slowly Oscillating Bodies of Revolution in Supersonic Flow," NASA TN D-3440, June 1966.

[8] Stahara, S. S. and Spreiter, J. R., "Unsteady Local Linearization Solution for Pulsating Bodies at $M_\infty = 1$," *AIAA Journal*, Vol. 14, July 1976, pp. 990-992.

[9] Abramowitz, M., and Stegun, I. A., *Handbook of Mathematical Functions*, National Bureau of Standards, 1966, p. 228.

[10] Spreiter, J. R. and Alksne, A., "Slender Body Theory Based on Approximate Solution of the Transonic Flow Equation," NASA TR R-2, 1959.

[11] Wehrend, W., Jr., "An Experimental Evaluation of Aerodynamic Damping Moments of Cones with Different Center of Rotation," NASA TN D-1768, 1963.

DEVELOPMENTS IN TRANSONIC STEADY AND UNSTEADY FLOW THEORY

John R. Spreiter
Stanford University
Stanford, California

and

Stephen S. Stahara
Nielsen Engineering & Research, Inc.
Mountain View, California

Abstract

Great strides have been made in recent years in the analysis of transonic flows past wings and bodies, and the initial extensions to wing-body combinations, helicopter rotors, and internal flow through rotating turbomachinery have been announced. Although the methods are too numerous and diverse to permit detailed description, the salient features and results of the more significant are reviwed.

I. Introduction

With the propsect of efficient transonic flight afforded by the development of supercritical airfoils providing the motivation, with the results [1-5] of a previous era extending from about 15 to 25 years ago providing the foundation, and with an enhanced computational capability providing the means, enormous progress in transonic flow analysis is currently being made. During this decade, several new methods particularly adapted for use with advanced computers have been developed to calculate flows about increasingly complex aerodynamic configurations. These techniques are not limited to the small disturbance theory that formed the basis for most of the earlier work, but apply also to (a) the complete potential equation for irrotational flow, (b) the Euler equations for general inviscid flow, and (c) even the Navier-Stokes equations for viscous flow. Some of the methods, such as the numerical time-dependent procedures, have been applied to all levels of description. Others, as the hodograph, are restricted to two-dimensional steady flow governed by either the complete potential equation or its small disturbance counterpart. Still others, as the integral equation method, have broader potentialities, but are presently developed primarily for the small disturbance equation. As might be expected, most methods have been applied to the small disturbance formulation and fewest to the Navier-Stokes equations. Under favorable circumstances, the various methods yield similar results, with the effects of viscosity being confined to limited regions, so that the results of the small disturbance theory agree with those of the more accurate theories. Some of the differences, moreover, stem directly from differences in computational details such as mesh size, order of accuracy of the difference algorithm, etc., and could be reduced at the expense of greater computing time or with the development of more effective algorithms.

Because the volume of material is so large, and reference can be made to several excellent reviews [6-11] as well as the original papers, our approach here is to provide a broad overview by combining brief accounts of the theoretical basis of the various methods followed by a presentation and discussion of significant results, usually obtained by more than one method. We start with two-dimensional flows, for which the number and variety of methods is greatest, and with the Navier-Stokes representation so that the initial results presented will provide a standard with which the following approximate theories can be judged. Three-dimensional flows are discussed subsequently.

II. Two-Dimensional Flow

Although the majority of analysis has been directed toward an inviscid level of approximation, transonic flows are often highly influenced by viscous phenomena, particularly shock-induced boundary-layer separation. The most complete analysis of such a flow is that of Diewert[12,13] who employs the finite volume method to solve the time-dependent, Reynolds-averaged Navier-Stokes equations which, written in integral form, are

$$\frac{\partial}{\partial t}\int_{vol}\begin{Bmatrix}\rho\\ \rho U\\ \rho W\\ E\end{Bmatrix} d\,vol + \int_{S}\begin{Bmatrix}\rho\underset{\sim}{q}\\ \rho U\underset{\sim}{q} + \bar{\tau}\cdot\hat{i}_x\\ \rho V\underset{\sim}{q} + \bar{\tau}\cdot\hat{i}_y\\ E\underset{\sim}{q} + \bar{\tau}\cdot\underset{\sim}{q} - \kappa\nabla T\end{Bmatrix}\cdot\hat{n}\,dS = 0 \qquad (1)$$

where

$$\underset{\sim}{q} = \hat{i}_x U + \hat{i}_z W,$$

$$\bar{\tau} = \hat{i}_x\hat{i}_x\sigma_x + \hat{i}_x\hat{i}_z\tau_{xz} + \hat{i}_z\hat{i}_x\tau_{zx} + \hat{i}_z\hat{i}_z\sigma_{zz}$$

in which ρ is density, U and W are velocity components and $\hat{i}_x$ and $\hat{i}_z$ are unit vectors parallel to the x and z axes, $E = e + (U^2 + V^2)/2$ is total energy per unit volume, κ is thermal conductivity, ∇T is temperature gradient, σ and τ are normal and shear stresses, and $\hat{n}$ is a unit normal vector. In addition to ordinary viscous stresses in τ, Diewert also includes turbulent Reynolds stresses estimated using four different algebraic eddy viscosity models. If the viscous and Reynolds stresses are disregard, Eq. (1) reduces to the integral form of the Euler equations for inviscid flow,

$$\frac{\partial}{\partial t}\int_{vol}\begin{Bmatrix}\rho\\ \rho U\\ \rho W\\ E\end{Bmatrix} d\,vol + \int_{S}\begin{Bmatrix}\rho\underset{\sim}{q}\\ \rho U\\ \rho W\\ E\end{Bmatrix}\underset{\sim}{q}\cdot\hat{n}\,dS + \int_{S}\begin{Bmatrix}0\\ p\,\hat{n}\\ p\,\hat{n}\\ p\,\underset{\sim}{q}\cdot\hat{n}\end{Bmatrix} dS = 0 \qquad (2)$$

The integral forms are appropriate for the finite volume method used by Diewert for viscous flow and also by Rizzi[14] for inviscid flow; but other methods are usually derived from the

corresponding differential equations. The Euler equations, for example, are as follows when written in conservation form to include the shock relations directly

$$\frac{\partial}{\partial t}\begin{Bmatrix}\rho\\ \rho U\\ \rho W\\ E\end{Bmatrix} + \frac{\partial}{\partial x}\begin{Bmatrix}\rho U\\ \rho U^2 + p\\ \rho UW\\ U(E+p)\end{Bmatrix} + \frac{\partial}{\partial z}\begin{Bmatrix}\rho W\\ \rho UW\\ \rho W^2 + p\\ W(E+p)\end{Bmatrix} = 0 \qquad (3)$$

Since these equations are difficult to solve, they are often approximated by assuming the flow to be isentropic. This is correct without approximation for flows which are continuous, i.e., shock-free, and a good approximation for flows with shock waves if they are not too strong. Under these circumstances,

$$(p/p_\infty)/(\rho/\rho_\infty)^\gamma = \exp\,[(s - s_\infty)/c_v] \qquad (4)$$

where $\gamma = c_p/c_v$ is the ratio of specific heats at constant volume and pressure, s is entropy, and subscript ∞ refers to free-stream conditions. Then Eq. (3) reduces to

$$\frac{\partial}{\partial t}\begin{Bmatrix}\rho\\ \rho U\\ \rho W\end{Bmatrix} + \frac{\partial}{\partial x}\begin{Bmatrix}\rho U\\ \rho U^2 + p_o(\rho/\rho_o)^\gamma\\ \rho UW\end{Bmatrix} + \frac{\partial}{\partial z}\begin{Bmatrix}\rho W\\ \rho UW\\ \rho W^2 + p_o(\rho/\rho_o)^\gamma\end{Bmatrix} = 0 \qquad (5)$$

Magnus and Yoshihara[15] have introduced time-dependent numerical methods to transonic analysis by solving these equations.

A related assumption, which is also exact for shock-free flow and a good approximation if the shock waves are not too strong, is that the flow is irrotational. There then exists a velocity potential Φ related to the velocity by $\underset{\sim}{q} = \nabla\Phi$ that satisfies

$$(a^2 - \Phi_x^2)\Phi_{xx} - 2\Phi_x\Phi_z\Phi_{xz} + (a^2 - \Phi_z^2)\Phi_{zz} - \Phi_{tt} - 2\Phi_x\Phi_{xt} - 2\Phi_z\Phi_{zt} = 0 \qquad (6)$$

where $a = [a_o^2 - (\gamma-1)q^2/2]^{1/2}$ is the local speed of sound, and a_o is the stagnation speed of sound. When applied to steady flow so that the time derivatives vanish, Eq. (6) is of elliptic type where the local Mach number $M = |\underset{\sim}{q}|/a < 1$, and hyperbolic type where $M = |\underset{\sim}{q}|/a > 1$. Both the hodograph and finite difference relaxation methods have been used extensively to solve this equation.

Most transonic analysis both past and present has, however, been based on a small disturbance approximation to Eq. (6). For flow with free-stream velocity $\underset{\sim}{q}_\infty = \hat{i}_x U_\infty$ past a thin airfoil aligned approximately with the x axis, a perturbation velocity potential $\phi = \Phi - U_\infty x$ can be introduced and shown to satisfy

$$(1 - M_\infty^2 - k\phi_x)\phi_{xx} + \phi_{zz} - \frac{2M_\infty^2}{U_\infty}\phi_{xt} - \frac{M_\infty^2}{U_\infty}\phi_{tt} = 0 \qquad (7)$$

For $M_\infty = U_\infty/a_\infty \neq 1$, a number of alternatives exist for k, but the widely used expression $k = (\gamma+1)M_\infty^2/U_\infty$ provides a good all-around compromise.

Equations (1) through (7) must be supplemented by boundary conditions and other relations to specify both a mathematical problem corresponding to a physical application and a unique solution. Boundary conditions must describe conditions at infinity and at the airfoil surface. With Eq. (1), the velocity must satisfy the no-slip condition at the airfoil surface; whereas only the normal component must match that of the airfoil surface with Eqs. (2) through (7). With Eq. (7), it is customary to linearize the boundary condition and transfer it to the x axis. Thus,

$$(\phi_z)_{z=0} = U_\infty\left(\frac{\partial Z}{\partial x} + \frac{1}{U_\infty}\frac{\partial Z}{\partial t}\right) \qquad (8)$$

for an airfoil having ordinates $Z(x,t)$. Similarly, the exact Bernoulli equation is used with Eq. (6), whereas an approximation

$$C_p = \frac{p - p_\infty}{\frac{\rho_\infty}{2}q_\infty^2} = -\frac{2}{U_\infty}\left(\phi_x + \frac{1}{U_\infty}\phi_t\right) \qquad (9)$$

is normally used with Eq. (7). Equations (1) through (5) do not need supplementary relations for shock waves, but Eqs. (6) and (7) do. To complete the specification for a lifting airfoil, it is also necessary to impose the Kutta condition or some counterpart.

Of the many methods for solving steady transonic flow problems, the hodograph method is unique in that it depends on a transformation that linearizes the governing equation without approximation by interchanging the dependent and independent variables. In this way, the steady-state form of Eq. (6) transforms to

$$(a^2 - U^2)\phi_{UU} - 2UW\,\phi_{UW} + (a^2 - W^2)\phi_{WW} = 0 \qquad (10)$$

and its small disturbance counterpart, Eq. (7), to

$$(1 - M_\infty^2 - ku)\phi_{ww} + \phi_{uu} = 0 \qquad (11)$$

in which ϕ is the Legendre potential related to the coordinates by $\phi_u = x$ and $\phi_w = z$. The Jacobian of the transformation, $J = u_x^2(M_\infty^2 - 1 + ku) - u_z^2$ in the case of Eq. (11), cannot vanish where the flow is subsonic, but may vanish where it is supersonic, thereby signifying an inconvenient multiple mapping in the hodograph plane of a single point in the physical plane. As a result, use of this method is usually confined to the subsonic region and a limited part of the supersonic region unless the latter is small as at slightly supercritical Mach numbers. The remainder of the solution is calculated by another method, such as characteristics or finite differences. The hodograph method was used extensively in the early development of transonic flow theory[2,4], but difficulties in imposing boundary conditions for an airfoil of specified shape restricted its usefulness. It has come into a new era of significance in the design of shock-free airfoils for which it is particularly well suited.

Two methods of solving the hodograph equations are currently predominant. That of Nieuwland[16], Takahashi[17], and Boerstoel[18] relies on function theory and integral transforms; that of Bauer, Garabedian, and Korn[19,20] is based on analytical continuation into the complex domain so that the solution can be obtained by solving initial value problems. Both methods culminate with extensive numerical computations.

The first method to be developed for shocked transonic flow that depends intrinsically on the modern electronic computer is the time-dependent method of Magnus and Yoshihara[15,21,22]. It applies a modified Lax-Wendroff difference scheme to Eq. (5) to compute from a knowledge of ρ, U, and W at one time new values for a slightly later time. Repetitive application provides a time history of the development of the flow from an assumed initial state. Solutions for steady flow are obtained by imposing steady boundary conditions and carrying the calculations sufficiently forward in time for the transients to disappear, characteristically a costly process.

Relaxation methods were used in the early transonic studies of Emmons[23] in physical variables and Vincenti and Wagoner[24,25] in hodograph variables, but modern applications derive directly from Murman and Cole[26] who introduced the use of different difference expressions in the subsonic and supersonic regions in conformity with the respective domains of influence. The procedure was initially applied to Eq. (10) in which ϕ_{zz} is approximated by centered differences; and ϕ_x and ϕ_{xx} are represented by centered differences in regions of subsonic flow and by one-sided upwind differences in regions of supersonic flow. The resulting large set of algebraic equations was solved numerically using a successive line overrelaxation (SLOR) procedure.

It was soon recognized that the use of only two types of operators for ϕ_x and ϕ_{xx} was insufficient since difficulties arose at the sonic line and shock wave where transitions between the two forms had to be made. The problem was resolved by introducing a sonic finite difference operator corresponding to the centered-difference expression for ϕ_{zz} and a shock operator corresponding to the sum of the subsonic and supersonic operators. The latter when applied to the steady-state form of Eq. (7) rewritten in conservation form

$$[1 - M_\infty^2 - (k/2)\phi_x^2]_x + (\phi_y)_y = 0 \qquad (12)$$

results in substantial improvement of the calculated changes across a shock wave[27]. Presently, two types of differencing procedures are widely used with regard to the small disturbance equation. To distinguish them, those employing the shock point operator (SPO), which assures conservation of mass at shock points, are designated FCR (fully conservative relaxation); while those which do not employ the SPO are termed NCR (not fully conservative relaxation). Further complications arise when the method is applied to the complete potential Eq. (6) specialized to steady flow. The centerline of the Mach forecone region of dependence in supersonic flow is no longer parallel to the x axis, but is in the local direction of the streamlines. The calculations fail to converge if the differencing is done in the same way as in the small disturbance theory since the region of dependence of the differencing scheme does not always include that of the differential equation. However, Jameson[28] showed that convergence could be achieved if the finite difference elements were rotated to allow for the change in direction.

Improvements have also been made in devising more efficient algorithms for solving the large set of algebraic equations provided by the finite difference procedure. The SLOR method employed originally has been supplemented by more efficient procedures[6,8,9,10,29,30], and further advances exploiting steadily improving computer capabilities are to be anticipated.

The integral equation method, stemming from Oswatitsch[31] and Spreiter and Alksne[32], was the first method capable of providing results with embedded shock waves for supercritical flows. In this method, Green's theorem is used to transform the steady-state form of Eq. (7) into a nonlinear integral equation

$$\bar{u} = \bar{u}_L + \nu\bar{u}^2 - \frac{1}{2\pi}\iint \frac{\bar{u}^2}{2}\,\frac{(\bar{x}-\bar{\xi})^2 - (\bar{z}-\bar{\zeta})^2}{[(\bar{x}-\bar{\xi})^2 + (\bar{z}-\bar{\zeta})^2]^2}\,d\bar{\xi}\,d\bar{\zeta} \qquad (13)$$

where $\bar{x} = x$, $\bar{z} = (1 - M_\infty^2)^{1/2} z$, $\bar{u} = u/u_{cr} = k\bar{u}/(1 - M_\infty^2)$, and u_L represents the solution of Eq. (7) with the nonlinear and time-derivative terms omitted. Originally, the singularity at the field point where $\bar{u}$ is to be evaluated was enclosed by an infinitesimal rectangle having a ratio λ of height to width of infinity, in which case $\nu = 1/2$. Nixon and Hancock[33] have subsequently obtained $\nu = 1/4$ by enclosing the same point by an infinitesimal circle. Ogana and Spreiter[34] have investigated this matter further by enclosing the field point in an infintesimal rectangle of arbitrary λ, for which $\nu = (1/\pi)\arctan\lambda$. This accounts for the earlier results since $\nu = 1/2$ when $\lambda = \infty$, and $\nu = 1/4$ when $\lambda = 1$. These differences are somewhat illusory, however, since the doublet integral is semi-convergent and its value depends on λ in such a way that the sum of the last two terms of Eq. (13) is independent of the shape of the contour.

Solutions of Eq. (13) were sought initially by introduction of a velocity profile f of the form $\bar{u}(\bar{x},\bar{z}) = \bar{u}(\bar{x},0)f(\bar{x},\bar{z},\bar{u}_{z=0},Z)$ so that the double integral could be approximated by a single integral and solutions could be obtained with a modest amount of hand computation[32,35]. Although this method has substantial merit[36], the trend[33,37] is to direct numerical solution. Nixon and Hancock[33] have shown, in addition, that a notable improvement for the vicinity of the leading edge may be achieved by using a modified $\bar{u}_L$ obtained by replacing the boundary condition of Eq. (8) with

$$(\phi_z)_{z=Z} = (U_\infty + \phi_x)_{z=Z}\,\frac{dZ}{dx} \qquad (14)$$

In addition to the above methods that may be refined systematically to provide an essentially exact solution within the framework of small disturbance theory, there are several approximate methods that can provide accurate results, often

very simply. Principal among these are the local linearization[38,39] and the parametric differentiation[40] methods Since they are not in such an active stage of development, no general description will be provided; although their results will be displayed for comparison.

We turn now to the results provided by all of the methods discussed. Figure 1 presents pressure distributions for an 18-percent thick circular-arc airfoil as measured[41], and as calculated by Diewert[12,13] for both inviscid and viscous flow

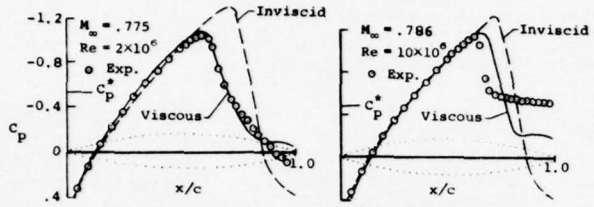

Fig. 1.- Pressure distributions for thick circular-arc airfoil.

by application of the finite volume method to Eq. (1). The inviscid solution agrees well with experiment over the forward half of the airfoil, but is inaccurate in predicting shock strength and location, and the pressure level near the trailing edge. When the aft pressure recovery is strong, as for Reynolds number, $Re = 2\times10^6$, the viscous solution agrees well with experiment. When the aft pressure recovery is weak, the theoretical results disagree, probably because of inadequate turbulent modeling in the separated region. At the present time, these are the most complete comparisons between viscous theory and experiment; the differences should be remembered in evaluating subsequent comparisons between inviscid theory and experiment.

Figure 2 presents a comparison of exact and approximate solutions for steady inviscid shock-free transonic flow past two different supercritical airfoils[10]. It shows that results obtained

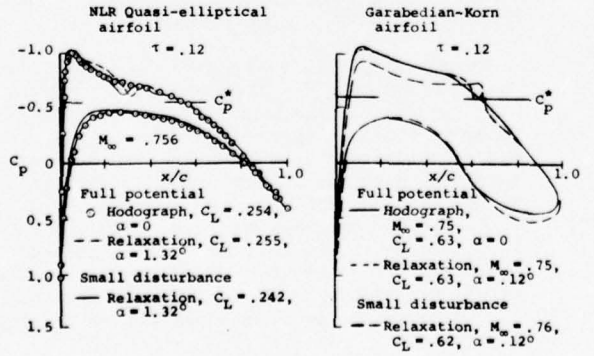

Fig. 2.- Theoretical shock-free pressure distributions for two supercritical airfoils.

by application of finite difference relaxation methods[42,43] to the complete potential Eq. (6), and the hodograph method[43,44] to its counterpart Eq. (10), are virtually identical; and, furthermore, that the transonic small disturbance Eq. (7)[45] can provide results of outstanding accuracy, a conclusion long evident from early studies[3].

Figure 3 from Ballhaus[9] shows pressure distributions for transonic flow with embedded shock wave for an NACA 64A410 airfoil calculated by application

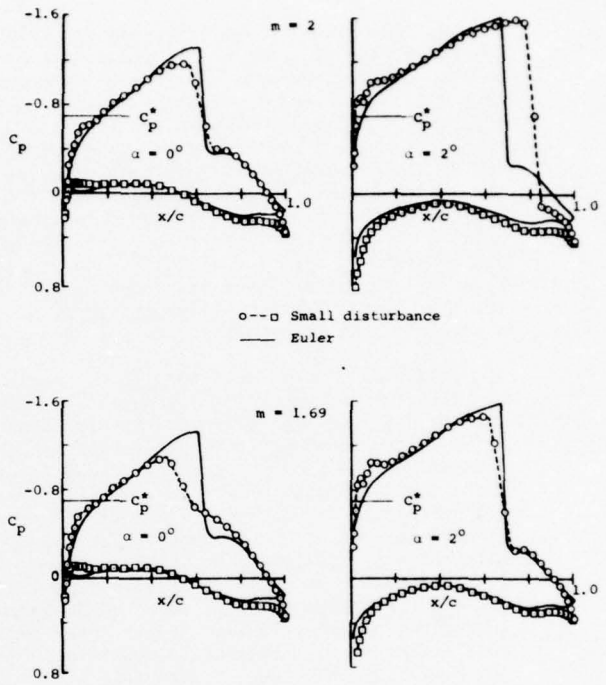

Fig. 3.- Exact and approximate transonic pressure distributions for an NACA 64A410 airfoil at two angles of attack, $M_\infty = 0.72$.

of the time-dependent method[15,21,22] to the Euler Eqs. (5) for isentropic flow and of the finite difference relaxation method to the small disturbance Eq. (7). Two versions of the latter are shown distinguished by the value of m in $k = M_\infty^m(\gamma+1)/U_\infty$. The upper plots are for $m = 2$, in wide use for many years[46]. To improve accuracy without complication Krupp[47] has proposed several other values for m, each of which has certain desirable properties such as the accuracy of the approximation for the shock jumps or the critical pressure coefficient, C_p^*. Among these values is $m = 1.69$ used in the lower plots of Fig. 3. The results illustrate the dilemma encountered in such efforts. The results for $m = 1.69$ are superior for angle of attack, $\alpha = 0$, but those for $m = 2$ are better for $\alpha = 2°$. To us, it seems preferable to use $m = 2$ for most applications, reserving other values for restricted classes of applications that emphasize a particular feature of the flow that can be better represented by another value for m.

As noted above, significant differences occur for the vicinity of a shock wave depending on whether the finite differencing is done with the FCR or NCR procedures. These are illustrated in Fig. 4 for a nonlifting 6-percent thick circular-arc airfoil at two different values for M_∞[27].

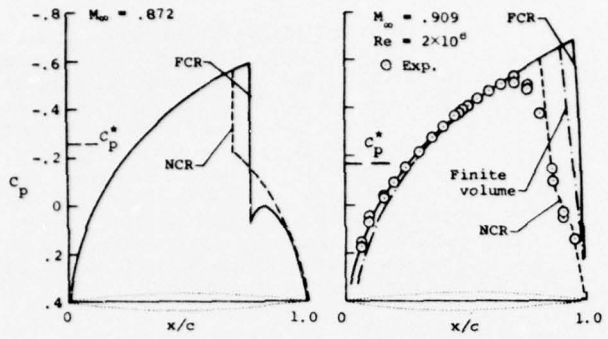

Fig. 4.- Supercritical pressure distributions for a thin circular-arc airfoil indicated by the FCR and NCR solutions of the transonic small disturbance equations, by the finite volume solution of the Euler equations, and by experiment.

Away from the shock wave, the results are in agreement, but near the shock wave they are quite different. In particular, the NCR shock pressure jump does not approach the theoretical normal shock jump; whereas the FCR solution shows not only that the correct condition is attained but that the shock is followed by a well-defined reexpansion, as is proper. The FCR solution also indicates a more downstream location for the shock wave than the NCR solution. Superposed on the results for $M_\infty = 0.909$ are experimental data[48] and a finite volume solution[14] of the Euler Eqs. (2). This comparison confirms that the FCR shock location agrees better with the exact inviscid location than the NCR locations; although the latter agree better with experiment. This paradox can be resolved by reference to Fig. 1 in which it is illustrated how viscous effects lead to a more upstream location of an embedded shock than indicated by inviscid theory. In addition to the differences in the surface pressures illustrated in Fig. 4, Newman and South[49] have shown that the streamlines downstream of the shock are displaced outward substantially and erroneously by the NCR method because of spurious mass addition at the shock. The FCR method avoids this deficiency by satisfying mass conservation everywhere.

Analogous results for the same airfoil in a slightly supersonic stream with $M_\infty = 1.15$ are shown in Fig. 5[10,27]. The calculations were performed using the two relaxation methods and also a finite-difference solution of the Euler Eqs.(5) by

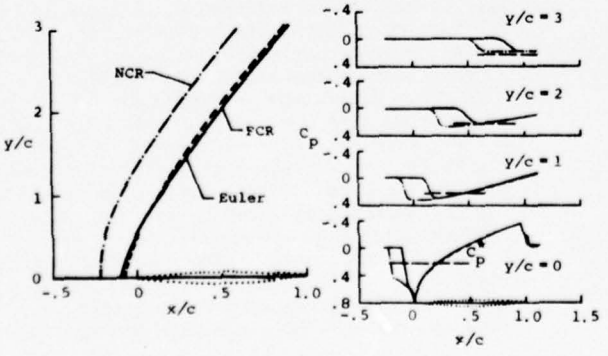

Fig. 5.- Pressure distributions and bow wave locations for a thin circular-arc airfoil indicated by FCR and NCR solutions of the transonic small disturbance equations, and an Euler solution.

a time-dependent method[50], which is fully conservative. All three methods indicate essentially the same pressure distribution on the airfoil, but the NCR method again indicates a location for the shock wave, this time detached, that is too far forward.

Although the integral equation method has been partially eclipsed by the hodograph and relaxation methods, recent reevaluations[33,36,37] indicate that it has considerable merit. Figure 6 shows pressure distributions for a 6-percent thick

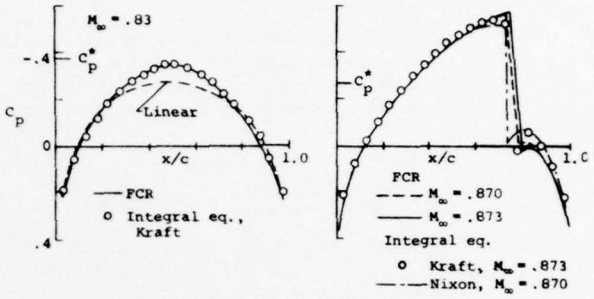

Fig. 6.- Pressure distributions for a 6-percent thick circular-arc airfoil indicated by integral equation and FCR solutions of the transonic small disturbance equation.

circular-arc airfoil calculated using two versions of the integral equation method and the small disturbance FCR finite difference method. The results of Kraft[36] have been determined using a velocity profile to reduce the doublet integral to a single integral and iterating in the manner of Spreiter and Alksne[32]. Those of Nixon[51] have been calculated using his extended integral equation method in which the doublet integral is evaluated by dividing the region of integration into a number of streamwise strips across which interpolation functions are used to express values for the integrand in terms of values along the strip edges. Similar results for the critical Mach number have also been determined by Ogana[37] who divided the region of integration into a large number of rectangles and evaluated the integral by quadrature at each step of an iteration process.

Corresponding results for a NACA 0012 airfoil are presented in Fig. 7 together with an essentially

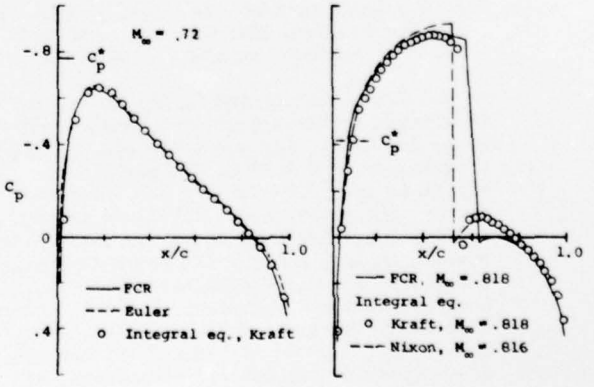

Fig. 7.- Pressure distributions for an NACA 0012 airfoil indicated by integral equation and FCR solutions of the transonic small disturbance equations, and by a numerical solution of the Euler equations.

exact solution of the Euler Eqs. (4)[52] for the subcritical case. The $x^{-1/2}$ singularity in u_L that would be present if the usual thin-airfoil boundary condition Eq. (8) were employed has been avoided in the integral equation results of Fig. 7 by using Eq. (14) for the boundary condition. Aside from modest differences near the shock, the integral equation results are virtually identical to those of the finite difference relaxation method and obtained with considerably less computation.

Attention is turned now to unsteady flow. Fig. 8 presents pressure distributions for an NACA 64A410 airfoil oscillating in pitch about a mean angle of attack of 2° in a flow with

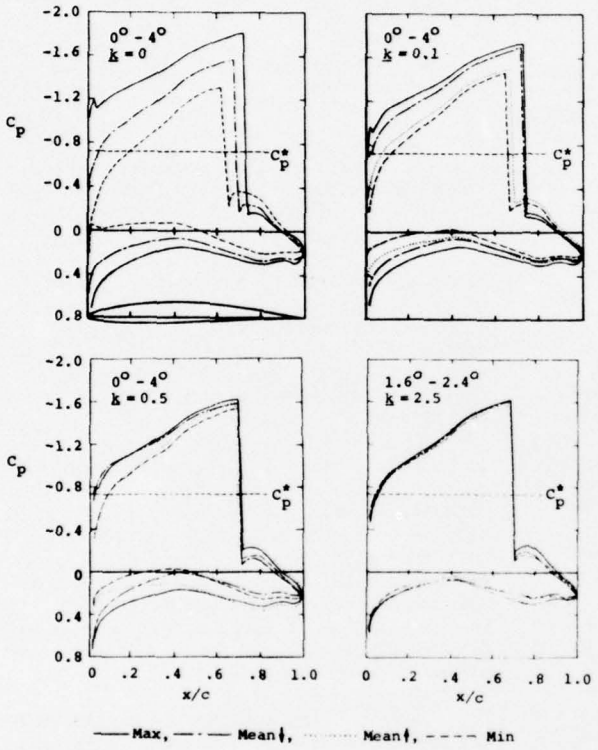

Fig. 8.- Time-dependent solution of Euler Eq. (5) for the pressure distribution on an NACA 64A410 airfoil oscillating in pitch.

$M_\infty = 0.72$, as calculated by Magnus and Yoshihara (21) using a time-dependent method to solve the Euler Eqs. (3). For the three smallest reduced frequencies $k = \omega c/2U_\infty$, the amplitude is 2°; but it is only 0.4° for $k = 2.5$. For each frequency, the pressure distributions on the upper and lower surfaces are shown for the minimum and maximum angles, and for the angle of attack both increasing and decreasing through the mean. At even the smallest frequency, $k = 0.1$, the results differ distinctly from those of quasi-stationary theory ($k = 0$). As k increases, the amplitude of the pressure variations diminishes, and the shock movement virtually vanishes for $k = 2.5$. The latter may be of importance to those developing approximate theories, since it suggests that shock movement may be disregarded for high frequency oscillations.

The results just described are of great theoretical significance; however, their computing cost is too high for the engineering analysis of aeroelastic and flutter problems which requires a large number of cases to be considered individually since solutions cannot be superposed. Simplification may be achieved by turning to the small disturbance theory for unsteady transonic flow, but the need to consider every case separately remains since Eq. (7) is nonlinear. For many applications, it is fruitful to decompose the problem into steady and unsteady components by letting

$$\phi = \bar{\phi} + \tilde{\phi}, \quad Z = \bar{Z} + \tilde{Z}, \quad C_p = \bar{C}_p + \tilde{C}_p \tag{15}$$

where the barred quantities satisfy Eqs. (7) through (9) with the time derivatives omitted. The remaining unsteady quantities should satisfy

$$(1 - M_\infty^2)\tilde{\phi}_{xx} - k(\bar{\phi}_x\tilde{\phi}_{xx} + \bar{\phi}_{xx}\tilde{\phi}_x + \tilde{\phi}_x\tilde{\phi}_{xx}) + \tilde{\phi}_{zz} - \frac{2M_\infty^2}{U_\infty}\tilde{\phi}_{xt} - \frac{M_\infty^2}{U_\infty^2}\tilde{\phi}_{tt} = 0 \tag{16}$$

for the boundary conditions and pressure relation given by Eqs. (8) and (9) with tildes over ϕ, Z, and C_p, but significant simplification can be achieved for small amplitude motions of an airfoil with nonvanishing steady-state disturbance field by disregarding $\tilde{\phi}_x\tilde{\phi}_{xx}$ to obtain a linear differential equation for $\tilde{\phi}$. Although the dependence of the variable coefficients $\bar{\phi}_x$ and $\bar{\phi}_{xx}$ on the nonlinear steady-state solution makes the equations more difficult to solve than those of ordinary linearized theory, $\tilde{C}_p$ is linearly dependent on the amplitude of the unsteady motion, and results for various unsteady motions about a single steady-state condition can be superposed to determine solutions for more complicated motions.

Fig. 9 presents results calculated in this way by Ehlers[53] using a finite difference relaxation method for an NACA 64A006 airfoil at zero angle of attack with an oscillating flap extending over the rear quarter chord. The results are qualitatively similar to the experimental data[54], but the unsteady pressures are generally overpredicted. Traci[55] et al., have confirmed Ehler's results by application of essentially the same method to the low frequency counterpart of Eq. (16) in which ϕ_{tt} is omitted in addition to the nonlinear term. Perhaps the most notable feature of the results is the unsteady pressure peak at about midchord in the supercritical example with $M_\infty = 0.853$ that is completely unheralded in the results for the subcritical example with $M_\infty = 0.794$. The peak at three-quarter chord is that normally expected at the hinge line for any subsonic flow. The second peak in the supercritical case is associated with the accumulation of receding waves as they move upstream from the flap until they are slowed and extensively refracted by the zone of supersonic flow. The data for $M_\infty = 0.90$ and 0.96 indicate that such effects disappear as expected when the flow upstream of the hinge line becomes supersonic.

Supplementing the development described above is a search for more economical approximate methods. Notable among these is an extension[56,57] of the local linearization method developed originally[39]

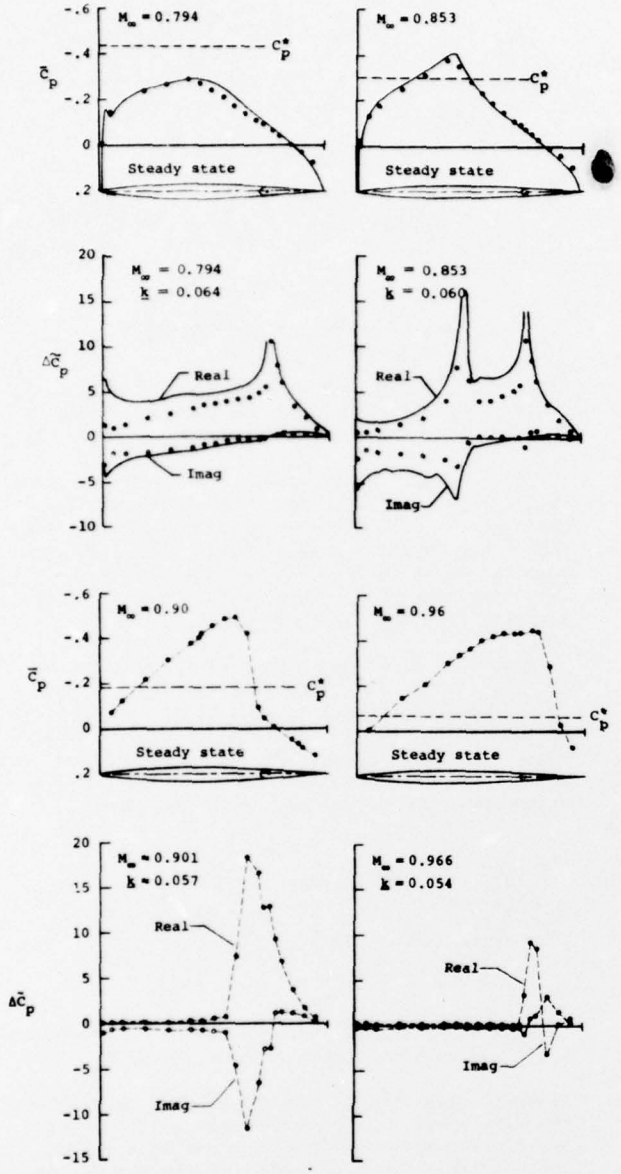

Fig. 9.- Pressure distributions on an NACA 64A006 airfoil with oscillating flap.

for steady flow. Results for the magnitude, $|\Delta\tilde{C}_p|$, and phase, $\Phi_{\tilde{C}_p}$, of the unsteady aerodynamic loading at $M_\infty = 1$ on a 6-percent thick circular-arc airfoil oscillating in pitch about the nose with ampltidue δ and various reduced frequencies $\underline{k}$ are shown in Fig. 10. Also included are the results of quasi-stationary theory and linearized theory to which the local linearization results converge for small and large $\underline{k}$. Rather similar results have been obtained by Isogai[58], Kimble and Wu[59], and Dowell[60] through application of somewhat different approximations based on the general notions of the local linearization method.

III. Axisymmetric and Related Slender-Body Flows

Several of the methods developed originally for two-dimensional flow have been extended to

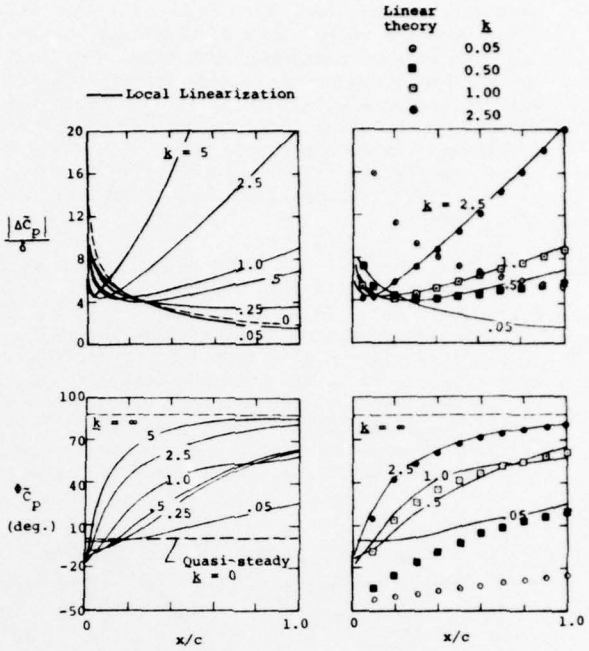

Fig. 10.- Load distribution on a thin circular-arc airfoil oscillating in pitch about the nose.

axisymmetric flow. Although some of the analyses have been based on the more complete theories, extensions to nonaxisymmetric slender bodies and wings have been confined almost exclusively to the small disturbance theory described by

$$(1 - M_\infty^2 - k\phi_x)\phi_{xx} + \phi_{yy} + \phi_{zz} - \frac{2M_\infty^2}{U_\infty}\phi_{xt} - \frac{M_\infty^2}{U_\infty}\phi_{tt} = 0 \quad (17)$$

together with appropriate boundary conditions, and a pressure relation modified to include $\phi_y^2 + \phi_z^2$ within the parentheses of Eq. (9).

Figure 11 shows pressure distributions for a 10-percent thick parabolic-arc body of revolution for several M_∞ from 0.9 to 1.1 calculated using the local linearization[61] and numerical NCR[62] methods together with experimental data[63]. These results, and also the previously unpublished FCR results calculated at NEAR, are in good agreement

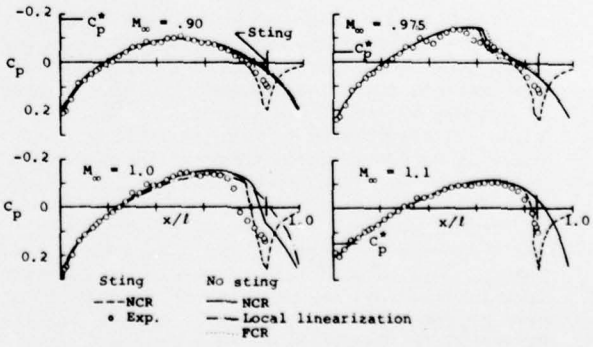

Fig. 11.- Pressure distributions for a parabolic-arc body of revolution indicated by various solutions of the small disturbance equations, and by experiment.

over most of the body, but notable differences exist near the rear. Some of these may be attributed to viscous phenomena, but effects of the cylindrical sting model support and wind tunnel walls are also significant. To demonstrate the effects of the sting, NCR results[62] are presented for a shape that conforms to the test model and sting combination. The results are in improved agreement with the data, but significant differences remain.

To investigate the effects of the walls, Bailey [62] carried out NCR calculations for the body-sting combination in a circular wind tunnel having the same cross-section area relative to the body as the Ames 14-foot wind tunnel where the tests were conducted. To simulate the ventilated walls of the test section, calculations were performed for a porous wall with various porosities. The results for a porosity of 0.5 are shown in Fig. 12 together with those for free air and for an open

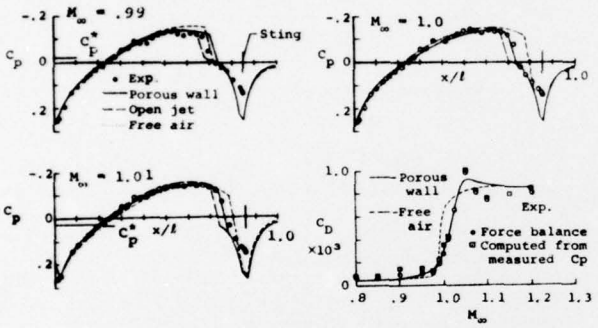

Fig. 12.- Pressure distributions and surface pressure drag for a parabolic-arc body of revolution with sting in free air, an open jet, and a wind tunnel with porous walls.

jet. Sedin and Karlsson[64] have obtained similar results for the porous wall using their alternating direction integration method. The theory indicates that the walls produce an upstream shift of the shock wave, thereby bringing the calculated pressure distribution and pressure drag into virtually perfect agreement with the measurements. Prudence should be exercised in accepting these results as definitive, however, since the boundary condition applied at the wall is a highly simplified representation of a complex local flow.

It has long been known[3] that the solution for certain thickness-dominated steady transonic flows past slender wings, bodies, and wing-body combinations can be decomposed into four simpler components by use of the transonic equivalence rule. As illustrated by Fig. 13 with ϕ_{xt} and $f(y,z,;x,t)$ set to zero, three of these require solution of only the two-dimensional Laplace equation for flows in each transverse y,z plane; and the fourth requires solution of the transonic small disturbance equation for axisymmetric flow past an "equivalent" body of revolution having the same longitudinal distribution of cross-section area as the original aerodynamic shape. Cheng and Hafez[65] and Barnwell[66] have extended that result to lift-dominated cases, for which it is necessary to include additional higher-order (multipole) inner solutions beyond the first-order thickness (source) and lift (dipole) solutions.

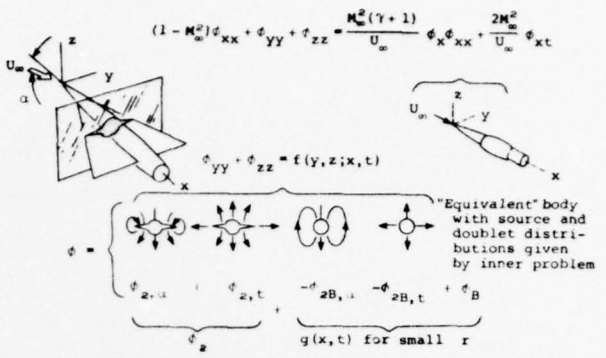

Fig. 13.- Schematic representation of unsteady transonic equivalence rule for slender wing-body combinations for mildly unsteady motions.

The first-order thickness and lift inner solutions satisfy the two-dimensional Laplace equation; but the higher-order solutions satisfy Poisson's equation in which the right-hand side $f(y,z;x)$ is a function of the lower-order solutions. We have recently extended the analysis to unsteady flows[57], arriving at the result portrayed in Fig. 13.

Figure 14 presents results of an application of the equivalence rule for steady flow with $M_\infty = 1$ to slender bodies with elliptic cross sections and the same longitudinal distribution of cross-section area as a parabolic-arc body of revolution of thickness ratio, 1/12[67]. The solution for the equivalent body was determined using the local

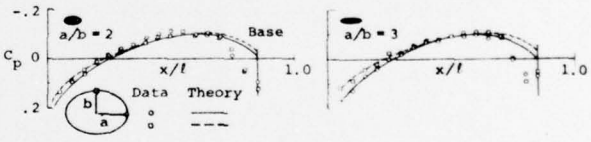

Fig. 14.- Pressure distributions on two parabolic-arc bodies of elliptic cross section; $M_\infty = 1$.

linearization method, the only method available at the time these results were originally published, and are for free-air flow past a complete body, i.e., without a sting. After making allowances for deficiencies over the rear of the body that can be attributed to effects of wind tunnel walls and model support, the results show that the equivalence rule provides a simple and accurate means for treating transonic flow past slender bodies of noncircular cross section.

Figure 15 presents a similar comparison of theoretical and experimental results for $M_\infty = 1$ for one of the elliptic cross-section bodies of Fig. 14 at angles of attack of 2°, 4°, and 6°[67]. Good agreement is again found along most of the body, with notable differences occurring on the rear. The latter could be rectified by replacing the solution for the equivalent body by a solution like that of Fig. 12 that accounts for effects of the model support and wind-tunnel walls.

In contrast to the foregoing, the development of methods for solving the nonlinear equations for unsteady axisymmetric and three-dimensional transonic flows has barely begun. We have applied the

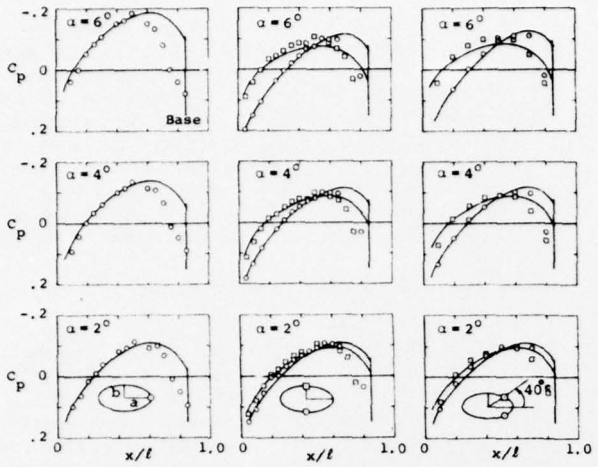

Fig. 15.- Pressure distributions on the body of Fig. 14 with a/b = 2 at three angles of attack, α; M_∞ = 1.

local linearization method to flow with $M_\infty = 1$ past a slender body of revolution engaged in a variety of unsteady motions. Fig. 16 reproduces results[57,68] for the amplitude and phase of the surface pressures on a nonlifting body undergoing

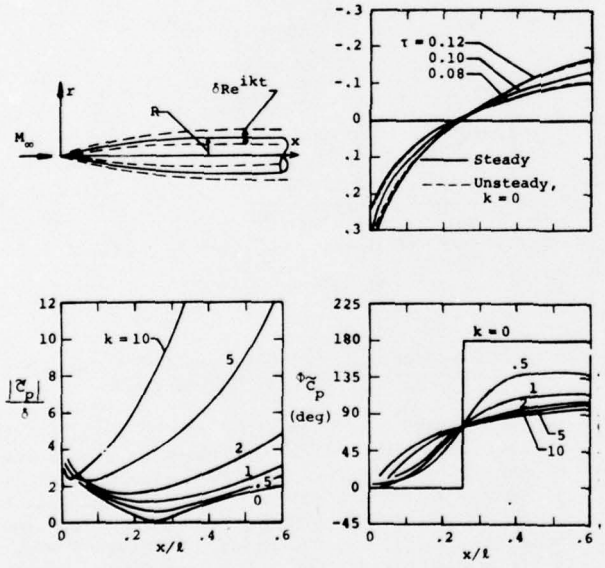

Fig. 16.- Local linearization solution for pressures on the forepart of a parabolic-arc body of revolution in oscillatory dilatation proportional to the local body radius; τ = 0.10, M_∞ = 1.

small oscillatory dilatations proportional to the local body radius. As in the two-dimensional applications, the results approach those of linearized theory for high frequency oscillations, and quasi-stationary theory for low frequencies. The latter is illustrated in the plot in the upper right in which the pressure distributions indicated by the unsteady analysis for a basic body of thickness ratio, τ = 0.10, undergoing slow expansion to τ = 0.12 and contraction to τ = 0.08 are shown to agree with local linearization solutions for steady flow past three such bodies. Extension of the local linearization analysis to the pitching motion of slender bodies of revolution at M_∞ = 1 has been carried out recently[69] and used to determine unsteady surface pressures and static and dynamic stability derivatives for conical and parabolic-arc bodies. The results are presented together with those of other approximate theories and are shown to agree well with available data.

IV. Three-Dimensional Flows Past Wings and Wing-Body Combinations

Much can be learned by the study of two-dimensional and slender-body flows, but rational aircraft design requires solutions for three-dimensional aerodynamic configurations. Fortunately, the finite difference relaxation method can be generalized to these situations, and modern computers are able to perform the computations in an acceptable time for steady flows past certain classes of three-dimensional shapes. To date, the analysis has been based almost exclusively on the small disturbance theory, which in its simplest form is described by Eq. 17 with ϕ_{xt} and ϕ_{tt} omitted.

Figures 17 and 18 present comparisons of calculated and experimental data for a swept ONERA M6 wing at an angle of attack of 3° for M_∞ = 0.84

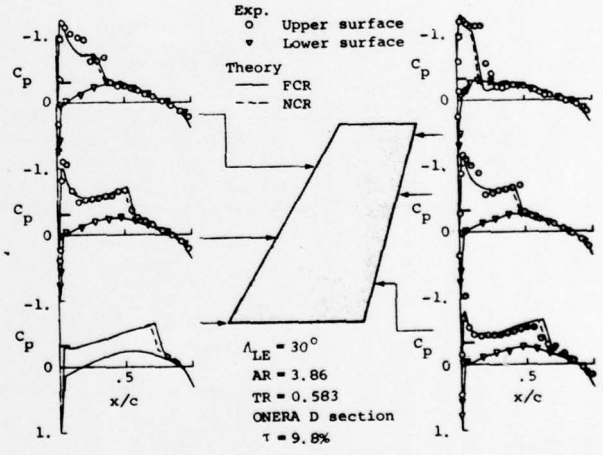

Fig. 17.- Pressure distributions on a swept ONERA M6 wing; M_∞ = 0.84, α = 3°.

and 0.93[70]. Computations were performed using both the NCR and FCR methods and required about 5 CPU minutes on the CDC 7600 computer. As in the two-dimensional applications, the FCR method predicts a more downstream location for the shock wave than the NCR method, with the difference being more marked at the higher Mach number. Again, the data agree better with the NCR calculations, but this is certainly due to a fortuitous cancellation of errors in the shock jumps by disregarded viscous effects.

The experimental data also reveal a weak oblique shock upstream of the main shock and swept back about 35°, but no indication of it is given by the calculations. This is to be expected because

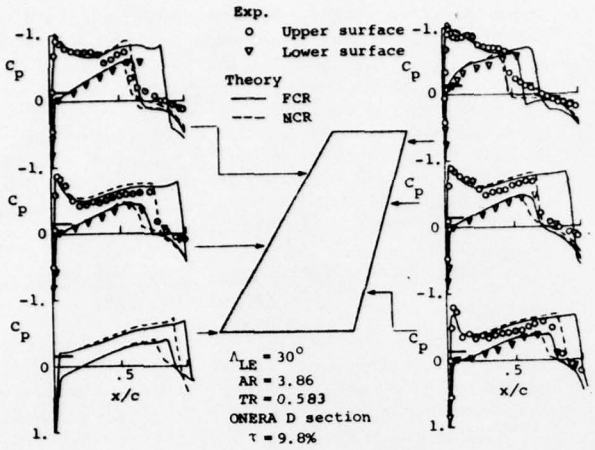

Fig. 18.- Pressure distributions on a swept ONERA M6 wing; $M_\infty = 0.93$, $\alpha = 3°$.

Eq. (17) provides a poor approximation for shocks with sweep angles greater than about 20°. A substantial improvement can be made, however, by adding two terms to Eq. (17) to obtain[10,71]

$$(1-M_\infty^2)\phi_{xx} + \phi_{yy} + \phi_{zz} = \frac{M_\infty^2(\gamma+1)}{U_\infty}\phi_x\phi_{xx} + \frac{M_\infty^2(\gamma-1)}{U_\infty}\phi_x\phi_{yy} + \frac{2M_\infty^2}{U_\infty}\phi_y\phi_{xy} \qquad (18)$$

for steady transonic flow. Studies of this and related extensions of the small disturbance theory are currently in progress. Moving closer to a complete airplane configuration, Fig. 19 presents experimental and NCR calculated pressures for a

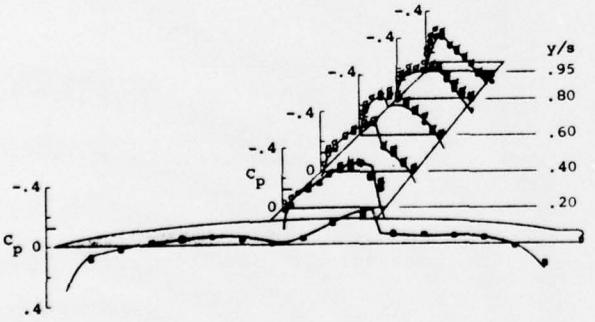

Fig. 19.- Pressure distribution on a wing-body combination; $M_\infty = 0.93$, $\alpha = 0°$.

swept-wing-fuselage configuration at $M_\infty = 0.93$ and $\alpha = 0°$[70]. The agreement with experiment is good along the fuselage centerline and the two inboard stations. In the computed results, the wing root shock propagates laterally to $y/s = 0.60$, but the experimental shock dissipates before reaching this point. The source of the disagreement is not clear but may be due to viscous effects or to deficiencies associated with swept shock waves.

As an alternative to the finite difference approach to three-dimensional transonic flow analysis, mention should be made of the alternating direction integration method of Sedin and Karlsson (64), which has recently been shown to be capable of providing plausible pressure distributions on wings and wing-body combinations. Further investigation of the accuracy and computational requirements of the method is necessary to determine its competitiveness with the finite difference methods.

V. Helicopter Rotors

The onset of transonic flow over the outer portion of the rotor blades is one of the primary conditions that sets the performance limits of modern helicopters. A transonic regime near a blade tip is inherently nonlinear, three-dimensional and, with forward flight, unsteady. As illustrated in Fig. 20(9), the shock on the upper surface moves downstream at points B and C, is nearly stationary at D, and moves upstream at E. Subsequently, the

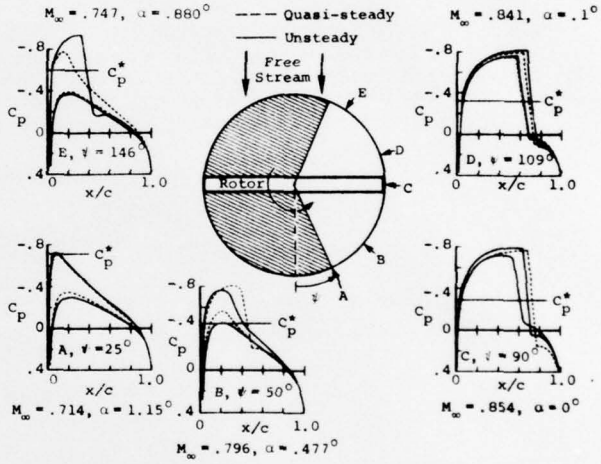

Fig. 20.- Pressure distributions for a simulated two-dimensional helicopter rotor.

shock propagates off the front of the airfoil into the oncoming flow. In the calculation of the theoretical results of Fig. 20, the unsteady motion of the rotor blade in forward flight was simulated by an NACA 0012 airfoil undergoing simultaneous sinusoidal Mach number and incidence variations with a phase difference of 180°. The governing equation is a two-dimensional low frequency version of Eq. (17) with ϕ_{yy} and ϕ_{tt} omitted and with $M_T + M_\infty \sin\psi$, which represents the instantaneous free-stream Mach number, in place of M_∞ in the coefficients of ϕ_{xt} and ϕ_{xx} and the boundary conditions. The quantity M_T is the tip Mach number due to rotation, and $\psi = \Omega t$ is the indicated azimuth angle on the rotor disk. The quasi-steady results were computed by solving the same equation with $\phi_{xt} = 0$, so that time appeared only as a parameter. The shaded region indicates the portion of the cycle for which the flow is subcritical, and for which the unsteady values for the pressures are nearly quasi-steady. In the supercritical region, however, the pressures and shock wave location lag the quasi-steady results.

The results of Fig. 20 correspond to strip theory, but three-dimensional effects are obviously important for a helicopter rotor, particularly near the tip. Caradonna and Isom[72] have investigated this feature of rotor aerodynamics, and calculated unsteady FCR solutions reproduced in Fig. 21 for both two- and three-dimensional representations.

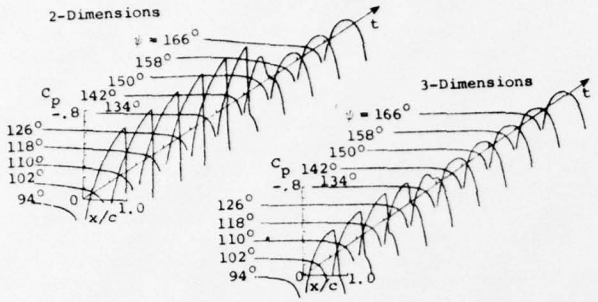

Fig. 21.- Two- and three-dimensional calculations of pressure distributions for several ψ at 97.7 percent of the rotor radius with blades of aspect ratio = 15 and 6-percent thick circular-arc profiles operating with an advance ratio, $U_\infty/\Omega R = 0.4$, and a tip Mach number, $M_T = 0.93$, at $\psi = 90°$.

Comparison shows that the three-dimensional solution indicates that the flow is far less expanded (the peak negative C_p is less in the supersonic region and the shock wave does not reach the trailing edge), the return to subsonic flow occurs earlier, and no upstream propagating wave is indicated for this case. Caradonna and Isom state that such a wave is seen in their results for a higher Mach number three-dimensional calculation, but its amplitude is about an order of magnitude less than indicated by the two-dimensional calculation. This brief account serves to indicate that helicopter aerodynamics provides a new field of application for transonic flow theory. The available results are very incomplete, but they illustrate the significance of transonic flow for helicopter rotors, and the need for a more comprehensive study.

VI. Rotating Turbomachinery

Flow through a high-speed fan or compressor is three dimensional, can include complex shock systems, and is unsteady even in a rotating frame of reference if a complete stage consisting of a rotor and stator or a fan preceded by inlet guide vanes is considered. Effects of viscosity and turbulence are important, particularly in the aft stages, and impact of the wake of one stage on the blades of the next is an important source of vibration and noise. The calculation of transonic flow through high-speed turbomachinery must be one of the most formidable problems in aerodynamics, but the technological need exists and methods are beginning to be developed.

In current work, the traditional approach is taken in which the inviscid flow field is considered first, leaving the viscous and turbulence effects to be added later, hopefully as small or localized perturbations. Since variations of pressure and flow direction may be substantial, the small disturbance theory is not expected to be as useful as it is for the external aerodynamics of the airplane. The appropriate equations for the inviscid analysis are, therefore, the Euler equations, or possibly the complete potential equation if the shock waves are not too strong. In the most advanced analysis, Erdos et al.,[73] have approximated the three-dimensional problem by a pair of two-dimensional problems, which are intended ultimately to be interacted to obtain the complete solution. Figure 22 presents the essential ideas of this decomposition and of the

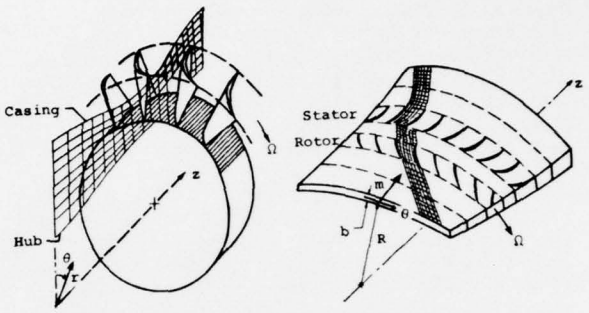

Fig. 22.- Coordinate systems and grid networks for interacting two-dimensional flows used to simulate three-dimensional flow through a rotor-stator stage of a turbomachine.

coordinate system evolved from it. The hub-to-casing solution accounts for effects of blockage of the flow area by the blades and the anticipated boundary layer as well as the geometry of the hub and casing, but not for any circumferential variations of the flow. It provides the flow properties in a meridional plane as averaged from one blade to the next, the coordinates $R = r(m)$ of the curved axisymmetric stream surface upon which the blade-to-blade analysis is carried out, and thereby the spacing $b(m)$ between two arbitrarily selected adjacent stream surfaces. The problem that must be solved for the blade-to-blade surface represents, therefore, a two-dimensional flow past a series of blades in the curvilinear coordinate system (m,θ) indicated in Fig. 22 with the radius, $R(m)$, and thickness, $b(m)$, of the stream sheet provided by the solution of the hub-to-casing solution. Expressed in a coordinate system rotating with the blades at an angular velocity Ω so as to obtain a steady flow problem if interaction with other blade rows is disregarded, the equations to be solved are

$$\frac{\partial \rho}{\partial t} + \frac{\partial(\rho V)}{R\partial\theta} + \frac{\partial(\rho U)}{\partial m} = -\frac{\rho U}{Rb}\frac{d(Rb)}{dm}$$

$$\frac{\partial(\rho V)}{\partial t} + \frac{\partial(p+\rho V^2)}{R\partial\theta} + \frac{\partial(\rho UV)}{\partial m} = -\frac{\rho UV}{Rb}\frac{d(Rb)}{dm} - \frac{\rho U}{R}(V+2\Omega R)\frac{dR}{dm}$$

$$\frac{\partial(\rho V)}{\partial t} + \frac{\partial(\rho UV)}{R\partial\theta} + \frac{\partial(p+\rho U^2)}{\partial m} = -\frac{\rho U^2}{Rb}\frac{d(Rb)}{dm} + \frac{\rho(V+\Omega R)^2}{R}\frac{dR}{dm}$$

$$\frac{\partial(\rho E_r)}{\partial t} + \frac{\partial(\rho V H_r)}{R\partial\theta} + \frac{\partial(\rho U H_r)}{\partial m} = -\frac{\rho U H_r}{Rb}\frac{d(Rb)}{dm} \qquad (19)$$

where U and V represent velocity components in the m and θ directions, and in which the relative total energy and total enthalpy are defined by

$$E_r = E - V\Omega R, \qquad H_r = H - V\Omega R \qquad (20)$$

The right-hand sides of Eq. (19), which differ from those of Erdos et al.[73] because of correction of errors in the transformation to curvilinear coordinates, arise from streamwise variations of thickness and radius of the stream sheet; they vanish if the equations are applied to a two-dimensional cascade flow. The corresponding equations for a nonrotating inertial system may be obtained by setting Ω to zero.

Only a few results obtained by solving these equations have been reported, and they are rather provisional because of the relatively small number of grid points used in the finite difference calculations. Results of blade-to-blade calculations of Erdos et al.,[73] are presented in Fig. 23 together with experimental data for a high-speed (1500-fps) fan tip section obtained

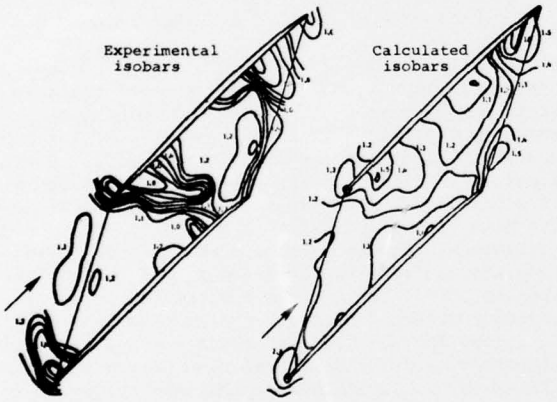

Fig. 23.- Experimental and calculated pressure distributions for flow through a 1500-fps rotor.

from an array of fast response pressure gages mounted on the casing wall. The test fan was preceded by a set of guide vanes and followed by a row of stators, but the unsteady interactions were neglected in the calculations and only the effects of the rotor was considered. Although the grid network was very coarse, the calculated flow bears a recognizable resemblance to the observations, particularly the indications of an oblique shock from the leading edge of the upper blade that reflects off the lower blade and reimpinges on the upper blade near the trailing edge. These developments give promise of substantial improvements in predictive capabilities for the design and analysis of high-speed turbomachinery. The flows are very complex, however, and continued effort will be required for some time before accurate and economical methods will be available for the routine solution of these problems.

VII. Concluding Remarks

The preceding discussion has provided a review of recent developments in steady and unsteady transonic aerodynamics. Many references are cited; but many significant contributions are not, or are hidden in references to summary papers. In many instances, the selection has been made on the basis of interlocking relations that help to evaluate the various results, and to provide a continuing base from which further discussion can proceed smoothly.

Overall, it is clear that tremendous advances are being made in the analysis of transonic flows, and that these problems no longer appear as formidable as they once did. Indeed, some of the simpler two-dimensional and axisymmetric steady flows may be considered solved, with even alternative methods available to choose among. The research frontier is moving now to more complex steady and unsteady three-dimensional flows past wings, wing-body combinations, helicopter rotors, and through turbomachinery fans and compressors. The modern computer has brought immense calculating power to bear on these problems, and the goal of replacing the wind tunnel with a computer is beginning to look more achievable than ever before. However, all will not fall into place by itself. Much work must be done, but the directions are indicated and the rewards of improved aerodynamic design and analysis are sufficient to demand the effort be made.

VIII. Acknowledgement

Acknowledgement is made for the support of this work to the Office of Naval Research under Contract N00014-73-C-0379/NR 061-215.

IX. References

1. von Kármán, T., "The Similarity Law of Transonic Flow," J. Math. & Phys., 16, 182-190, 1947.

2. Guderley, K. G., Theorie schallnaher Strömungen, Springer, 1957. Available in transl. (by J.R. Moszynski) as The Theory of Transonic Flow, Addison-Wesley, 1962.

3. Spreiter, J. R., "Aerodynamics of Wings and Bodies at Transonic Speeds," J. Aero/Space Sci., 26, 465-487, 1959.

4. Ferrari, C., and Tricomi, F. G., Aerodinamica Transonica, Edizioni Cremonese, 1962. Available in transl. (by R.H. Cramer) as Transonic Aerodynamics, Academic Press, 1968.

5. Oswatitsch, K., (Ed.), Symposium Transsonicum, Springer, 1964.

6. Oswatitsch, K., and Rues, D., Symposium Transsonicum II, Springer, 1976.

7. Jameson, A., "Transonic Flow Calculations," von Kármán Institute Lecture Series on Computational Fluid Dynamics, 1976.

8. Murman, E. M., (Ed.), Transonic Aerodynamics, AIAA Prof. Study Series, 1975.

9. Ballhaus, W. F., "Some Recent Progress in Transonic Flow Computation," von Kármán Institute Lecture Series on Computational Fluid Dynamics, 1976.

10. Bailey, F. R., "On the Computation of Two- and Three-Dimensional Steady Transonic Flows by Relaxation Methods," von Kármán Institute Lecture Series on Progress in Numerical Fluid Dynamics, 1974.

11. Wu, J. M., and Moulden, T. H., "A Survey of Transonic Aerodynamics," AIAA Paper No. 76-326, 1976.

12. Diewert, G. S., "Numerical Simulation of High Reynolds Number Transonic Flow," AIAA Jour., 13, 1354-1359, 1975.

13. Diewert, G. S., "Computation of Separated Transonic Turbulent Flow," AIAA Jour., 14, 735-740, 1976.

14. Rizzi, A., "Transonic Solutions of the Euler Equations by the Finite Volume Method," Symposium Transsonicum II, (Ed., K. Oswatitsch and D. Rues), Springer, 1976.

15. Magnus, R., and Yoshihara, H., "Inviscid Transonic Flow over Airfoils," AIAA Jour., 8, 2157-2162, 1970.

16. Nieuwland, G. Y., "Transonic Potential Flow Around a Family of Quasi-Elliptical Aerofoil Sections," NLR TR 172, 1967.

17. Takanashi, S., "A Method of Obtaining Transonic Shock-Free Flow Around Lifting Aerofoils," Trans. Japan Soc. Aero. Space Sci., 16, 34- , 1973.

18. Boerstoel, J. W., "Review of the Application of Hodograph Theory to Transonic Aerofoil Design and Theoretical and Experimental Analysis of Shock-Free Aerofoils," Symposium Transsonicum II, (Ed., K. Oswatitsch and D. Rues), Springer, 1976.

19. Bauer, F., Garabedian, P., and Korn, D., Supercritical Wing Sections, Lecture Notes in Economics and Mathematicel Systems, 66, Springer, 1972.

20. Bauer, F., Garabedian, P., Korn, D., and Jameson, A., Supercritical Wing Sections II, Lecture 108, Springer, 1975.

21. Magnus, R., and Yoshihara, H., "Finite Difference Calculations of the NACA 64A-410 Airfoil Oscillating Sinusoidally in Pitch at $M_\infty = 0.72$," Tech. Dept. CASD-NSC-74004, Convair Div. of Gen. Dyn., 1974.

22. Yoshihara, H., "A Survey of Computational Methods of 2D and 3D Transonic Flows with Shocks," GDCA-ERR-1726, Convair Aerospace Div. of Gen. Dyn., 1972. Also available in Transonic Aerodynamics, (Ed. E. M. Murman), AIAA Prof. Study Series, 1975.

23. Emmons, H. W., "Flow of a Compressible Fluid Past a Symmetrical Airfoil in a Wind Tunnel and in Free Air," NACA TN 1746, 1948.

24. Vincenti, W. G., and Wagoner, C. B., "Transonic Flow Past a Wedge Profile with Detached Bow Wave," NACA Rep. 1095, 1952.

25. Vincenti, W. G., Wagoner, C. B., and Fisher, N. H. Jr., "Calculations of the Flow Over an Inclined Flat Plate at Free Stream Mach Number One," NACA TN 3723, 1956.

26. Murman, E. M., and Cole, J. D., "Calculation of Plane Steady Transonic Flows," AIAA Jour., 9, 114-121, 1971.

27. Murman, E. M., "Analysis of Embedded Shock Waves Calculated by Relaxation Methods," AIAA Jour., 12, 626-633, 1974.

28. Jameson, A., "Iterative Solution of Transonic Flows Over Airfoils and Wings, Including Flows at Mach 1," Commun. Pure Appl. Math., 27, 283-309, 1974.

29. Martin, E. D., "A Fast Semidirect Method for Computing Transonic Aerodynamic Flows," Proc. AIAA 2nd Computational Fluid Dynamics Conf., 1975.

30. Ballhaus, W. F., and Steger, J. L., "Implicit Approximate-Factorization Schemes for the Low-Frequency Transonic Equation," NASA TM X-73,082, 1975.

31. Oswatitsch, K., "Die Geschwindigkeitsverteilung an symmetrischen Profilen beim Auftreten lokaler Überschallgebiete," Acta Physica Austriaca, 4, 228-271, 1950.

32. Spreiter, J. R., and Alksne, A. Y., "Theoretical Prediction of Pressure Distributions on Nonlifting Airfoils at High Subsonic Speeds," NACA Rep. 1217, 1955.

33. Nixon, D., and Hancock, G. J., "Integral Equation Methods - a Reappraisal," Symposium Transsonicum II, (Ed., K. Oswatitsch and D. Rues), Springer, 1976.

34. Ogana, W., and Spreiter, J. R., "Derivation of an Integral Equation for Transonic Flows," Submitted to AIAA Jour., 1975.

35. Spreiter, J. R., Alksne, A. Y., and Hyett, B. J., "Theoretical Pressure Distributions for Several Related Nonlifting Airfoils at High Subsonic Speeds," NACA TN 4148, 1958.

36. Kraft, E. M., "An Integral Equation Method for Boundary Interference in Perforated-Wall Wind Tunnels at Transonic Speeds," Ph.D. Dissertation, Univ. Tenn., 1975.

37. Ogana, W., "Computation of Steady Two-Dimensional Transonic Flows by an Integral Equation Method," Ph.D. Dissertation, Stanford Univ., 1975.

38. Spreiter, J. R., and Alksne, A. Y., "Thin Airfoil Theory Based on Approximate Solution of the Transonic Flow Equation," NACA Rep. 1359, 1958.

39. Spreiter, J. R., "The Local Linearization Method in Transonic Flow Theory," Symposium Transsonicum, (Ed., K. Oswatitsch), Springer, 1964.

40. Rubbert, P., and Landahl, M., "Solution of the Transonic Airfoil Problem Through Parametric Differentiation," AIAA Jour., 5, 470-479, 1967.

41. McDevitt, J. B., Levy, L. L., Jr., and Diewert, G. S., "Transonic Flow About a Thick Circular-Arc Airfoil," AIAA Jour., 14, 606-613, 1976.

42. Steger, J. L., and Lomax, H., "Transonic Flow About Two-Dimensional Airfoils by Relaxation Procedures," AIAA Jour., 10, 1972.

43. Garabedian, P. R., and Korn, D. G., "Analysis of Transonic Airfoils," Commun. Pure Appl. Math., 14, 841-851, 1973.

44. Lock, R. C., "Test Cases for Numerical Methods in Two-Dimensional Transonic Flows," AGARD Rept. NO1 575, 1970.

45. Krupp. J. A., and Murman, E. M., "The Numerical Calculation of Steady Transonic Flows Past Thin Lifting Airfoils and Slender Bodies," AIAA Paper No. 71-566, 1971.

46. Spreiter, J. R., "On the Application of Transonic Similarity Rules to Wings of Finite Span," NACA Rep. 1153, 1953.

47. Krupp, J. A., "The Numerical Calculation of Plane Steady Transonic Flows Past Thin Lifting Airfoils," Boeing Scientific Research Lab. Rep. D180-12958-1, 1971.

48. Knechtel, E. D., "Experimental Investigation at Transonic Speeds of Pressure Distributions over Wedge and Circular-Arc Airfoil Sections and Evaluations of Perforated-Wall Interference," NASA TN D-15, 1959.

49. Newman, P. A., and South, J. C., Jr., "Conservative Versus Nonconservative Differencing: Transonic Streamline Shape Effects," NASA TM X-72827, 1976.

50. Magnus, R. M., "The Direct Comparison of the Relaxation Method and the Pseudo-Unsteady Finite Difference Method for Calculating Steady Planar Transonic Flow," TN-73-SP03, Convair Aerospace Div. of Gen. Dyn., 1973.

51. Nixon, D., "Calculation of Transonic Flows Using an Extended Integral Equation Method," AIAA Paper No. 75-876, 1975.

52. Sells, C. C. L., "Plane Subcritical Flow Past a Lifting Airfoil," Proc. Roy. Soc., London, 308 (Series A), 377-401, 1968.

53. Ehlers, F. E., "A Finite Difference Method for the Solution of the Transonic Flow Around Harmonically Oscillating Wings," NASA CR-2257, 1975.

54. Tijdeman, H., and Schippers, P., "Results of Pressure Measurements of an Airfoil with Oscillating Flap in Two-Dimensional High Subsonic and Transonic Flow (Zero Incidence and Zero Mean Flap Position)," NLR TR 73078 U, 1973.

55. Traci, R. M., Albano, E. D., Farr, J. L., Jr., and Cheng, H. K., "Small Disturbance Transonic Flows About Oscillating Airfoils," AFFDL-TR-74-37, 1974.

56. Stahara, S. S., and Spreiter, J. R., "Development of a Nonlinear Unsteady Transonic Flow Theory," NASA CR-2258, 1973.

57. Spreiter, J. R., and Stahara, S. S., "Unsteady Transonic Aerodynamics - An Aeronautical Challenge," Unsteady Aerodynamics, (Ed., R. B. Kinney), Univ. Ar., 1975.

58. Isogai, K., "Unsteady Transonic Flow Over Oscillating Circular-Arc Airfoils," AIAA Paper No. 74-360, 1974.

59. Kimble, K. R., and Wu, J. M., "An Approximate Solution of Unsteady Transonic Flow Problems," AFFDL-TR-74-32, 1974.

60. Dowell, E. H., "A Simplified Theory of Oscillating Airfoils in Transonic Flow," Unsteady Aerodynamics, (Ed., R. B. Kinney), Univ. Ar., 1975.

61. Spreiter, J. R., and Alksne, A. Y., "Slender Body Theory Based on Approximate Solution of the Transonic Flow Equation," NASA Rep. R-2, 1959.

62. Bailey, F. R., "Numerical Calculation of Transonic Flow About Slender Bodies of Revolution," NASA TN D-6582, 1971.

63. Taylor, R. A., and McDevitt, J. B., "Pressure Distributions at Transonic Speeds for Parabolic-Arc Bodies of Revolution Having Fineness Ratios of 10, 12, and 14," NACA TN 4234, 1958.

64. Sedin, Y. c-J., and Karlsson, K. R., "Some Numerical Results of a New Three-Dimensional Transonic Flow Method," Symposium Transsonicum II, (Ed., K. Oswatitsch and D. Rues), Springer, 1975.

65. Cheng, H. K., and Hafez, M. M., "Transonic Equivalence Rule: A Nonlinear Problem Involving Lift," J. Fluid Mech., 72, 161-187, 1975.

66. Barnwell, R. W., "Transonic Flow About Lifting Configurations," AIAA Jour., 11, 764-766, 1973.

67. Spreiter, J. R., and Stahara, S. S., "Aerodynamics of Slender Bodies and Wing-Body Combinations at $M_\infty = 1$," AIAA Jour., 9, 1784-1791, 1971.

68. Stahara, S. S., and Spreiter, J. R., "Unsteady Local Linearization Solution for Dilatory Oscillation of Bodies of Revolution at $M_\infty = 1$," AIAA Jour., 14, 990-992, 1976.

69. Stahara, S. S., and Spreiter, J. R., "Unsteady Local Linearization Solution for Pitching Bodies of Revolution at $M_\infty = 1$: Stability Derivative Analysis," AIAA Jour. (in press).

70. Bailey, F. R., and Ballhaus, W. F., "Comparisons of Computed and Experimental Pressures for Transonic Flows About Isolated Wings and Wing-Fuselage Configurations," NASA SP-347, 1975.

71. Lock, R. C., "Research in the UK on Finite Difference Methods for Computing Steady Transonic Flows," Symposium Transsonicum II, (Ed., K. Oswatitsch and D. Rues), Springer, 1975.

72. Caradonna, F. X., and Isom, M. P., "Numerical Calculation of Unsteady Transonic Potential Flow over Helicopter Rotor Blades," AIAA Jour., 14, 482-488, 1976.

73. Erdos, J., Alzner, E., Kalben, P., McNally, W., and Slutsky, S., "Time-Dependent Transonic Flow Solutions for Axial Turbomachinery," NASA SP-347, 1975.

DISTRIBUTION LIST FOR UNCLASSIFIED TECHNICAL REPORTS AND REPRINTS ISSUED UNDER CONTRACT N00014-73-C-0379 TASK 061-215

Technical Library
Building 313
Ballistic Research Laboratories
Aberdeen Proving Ground, MD 21005

Dr. F. D. Bennett
External Ballistic Laboratory
Ballistic Research Laboratories
Aberdeen Proving Ground, MD 21005

Mr. C. C. Hudson
Sandia Corporation
Sandia Base
Albuquerque, NM 81115

Dr. J. D. Shreve, Jr.
Sandia Corporation
Sandia Base
Albuquerque, NM 81115

Defense Documentation Center
Cameron Station, Building 5
Alexandria, VA 22314 (12 copies)

Library
Naval Academy
Annapolis, MD 21402

Conductron Corporation
3475 Plymouth Road
P. O. Box 614
Ann Arbor, MI 48107

Air Force Office of Scientific Research (SREM)
1400 Wilson Boulevard
Arlington, VA 22209

Dr. G. H. Heilmeir, Director
Defense Advanced Research Projects Agency
1400 Wilson Boulevard
Arlington, VA 22209

Dr. R. Hoglund
Tactical Technology Office
Defense Advanced Research Projects Agency
1400 Wilson Boulevard
Arlington, VA 22209

Mr. J. L. Potter
Manager, VKF-AP
Arnold Air Force Station, TN 37389

Professor James C. Wu
School of Aerospace Engineering
Georgia Institute of Technology
Atlanta, GA 30332

Mr. M. J. Thompson
Defense Research Laboratory
University of Texas
P. O. Box 8029
Austin, TX 78712

Library
Aerojet-General Corporation
6352 N. Irwindale Avenue
Azusa, CA 91702

Dr. S. A. Berger
Department of Mechanical Engineering
University of California
Berkeley, CA 94720

Professor M. Holt
Department of Mechanical Engineering
University of California
Berkeley, CA 94720

Professor A. J. Chorin
Department of Mathematics
University of California
Berkeley, CA 94720

Dr. L. Talbot
Department of Mechanical Engineering
University of California
Berkeley, CA 94720

Dr. G. R. Inger
Department of Aerospace Engineering
Virginia Polytechnic Institute
Blacksburg, VA 24061

Professor A. H. Nayfeh
Department of Engineering Mechanics
Virginia Polytechnical Institute
Blacksburg, VA 24061

School of Applied Mathematics
Indiana University
Bloomington, IN 47401

Director
Office of Naval Research Branch Office
495 Summer Street
Boston, MA 02210

Supervisor, Technical Library Section
Thiokol Chemical Corporation
Wasatch Division
Brigham City, UT 84302

Dr. J. C. Erickson, Jr.
Calspan Corporation
P. O. Box 235
Buffalo, NY 14221

Mr. R. J. Vidal
Calspan Corporation
P. O. Box 235
Buffalo, NY 14221

Dr. Gordon Hall
Faculty of Engineering and Applied Sciences
Department of Mechanical Engineering
State University of New York at Buffalo
Buffalo, NY 14214

Professor R. F. Probstein
Department of Mechanical Engineering
Massachusetts Institute of Technology
Cambridge, MA 02139

Dr. John D. Anderson, Jr.
Chairman, Department of Aerospace Engineering
College of Engineering
University of Maryland
College Park, MD 20742

Professor W. L. Melnick
Department of Aerospace Engineering
University of Maryland
College Park, MD 20742

NASA Scientific and Technical Information Facility
P. O. Box 8757
Baltimore/Washington International Airport
Maryland 21240

Director
Office of Naval Research Branch Office
536 South Clark Street
Chicago, IL 60605

Code 753
Naval Weapons Center
China Lake, CA 93555

Professor R. T. Davis
Department of Aerospace Engineering and Applied Mechanics
University of Cincinnati
Cincinnati, OH 45221

Library MS 60-3
NASA Lewis Research Center
21000 Brookpark Road
Cleveland, OH 44135

Battelle-Defender Information Analysis Center
Battelle Memorial Institute
505 King Avenue
Columbus, OH 43201

Professor O. Burggraf
Department of Aeronautical and Astronautical Engineering
Ohio State University
Columbus, OH 43220

*Note: All addressees receive one copy unless otherwise specified.

Technical Library
Naval Surface Weapons Center
Dahlgren Laboratory
Dahlgren, VA 22418

Technical Library 2-51131
LTV Aerospace Corporation
P. O. Box 5907
Dallas, TX 75222

North American Aviation, Inc.
Space and Information Systems Division
12214 Lakewood Boulevard
Downey, CA 90240

U. S. Army Research Office
P. O. Box 12211
Research Triangle, NC 27709

Library, United Aircraft Corporation
Research Laboratories
Silver Lane
East Hartford, CT 06108

Dr. W. R. Briley
United Aircraft Corporation Research
Laboratory
East Hartford, CT 06108

Technical Library
AVCO-Everett Research Laboratory
2385 Revere Beach Parkway
Everett, MA 02149

Dr. Martin H. Bloom
Polytechnic Institute of New York
Department of Aerospace Engineering
and Applied Mechanics
Farmingdale, NY 11735

Technical Documents Center
Army Mobility Equipment R&D Center
Building 315
Fort Belvoir, VA 22060

Library (MS 185)
NASA Langley Research Center
Langley Station
Hampton, VA 23365

Code 2627
Naval Research Laboratory
Washington, DC 20375 (6 copies)

Dr. S. Nadir
Northrop Corporation
Aircraft Division
3901 West Broadway
Hawthorne, CA 90250

Professor Allen Chapmann, Chairman
Mechanical Engineering Department
William M. Rice Institute
Box 1892
Houston, TX 77001

Dr. Frank Lane
KLD Associates, Inc.
7 High Street
Huntington, NY 11743

Technical Library
Naval Ordnance Station
Indian Head, MD 20640

Professor E. L. Resler
Graduate School of Aerospace Engineering
Cornell University
Ithaca, NY 14850

Professor W. R. Sears
Aerospace and Mechanical Engineering
University of Arizona
Tucson, AZ 85721

Professor S. F. Shen
Graduate School of Aerospace Engineering
Cornell University
Ithaca, NY 14850

Library
Midwest Research Institute
425 Volker Boulevard
Kansas City, MO 64110

Dr. Robert Goulard
School of Aeronautics, Astronautics
and Engineering Sciences
Purdue University
Lafayette, IN 47907

Dr. N. C. Freeman
Aeronautics Department
Imperial College
London, S.W.7., England

Mr. John L. Hess
Douglas Aircraft Company
3855 Lakewood Boulevard
Long Beach, CA 90801

Dr. H. K. Cheng
Department of Aeropsace Engineering
University of Southern California
University Park
Los Angeles, CA 90007

Engineering Library
University of Southern California
Box 77929
Los Angeles, CA 90007

Dr. T. D. Taylor
The Aerospace Corporation
Post Office Box 95085
Los Angeles, CA 90045

Commanding Officer
Naval Ordnance Station
Louisville, KY 40214

Dr. C. Cook
Stanford Research Institute
Menlo Park, CA 94025

Professor E. R. G. Eckert
241 Mechanical Engineering Building
University of Minnesota
Minneapolis, MN 55455

Library
Naval Postgraduate School
Monterey, CA 93940

Supersonic-Gas Dynamics Research Lab.
Department of Mechanical Engineering
McGill University
Montreal 12, Quebec, Canada

Librarian
Engineering Library, 127-223
Radio Corporation of America
Morristown, NJ 08057

Dr. A. L. Slafkosky
Scientific Advisor
Commandant of the Marine Corps
(Code AX)
Washington, DC 20380

Dr. J. R. Spreiter
Nielsen Engineering & Research, Inc.
850 Maude Avenue
Mountain View, CA 94040

Engineering Societies Library
345 East 47th Street
New York, NY 10017

Dr. R. Vaglio-Laurin
Department of Aeronautics and
Astronautics
Polytechnic Institute of New York
New York, NY 10453

Professor S. Weinbaum
Department of Mechanical Engineering
The City University of New York
New York, NY 10031

Office of Naval Research
New York Area Office
715 Broadway - 5th Floor
New York, NY 10003

Librarian, Aeronautical Library
National Research Council
Montreal Road
Ottawa 7, Canada

Lockheed Missiles and Space Company
Technical Information Center
3251 Hanover Street
Palo Alto, CA 94301

Director
Office of Naval Research Branch Office
1030 E. Green Street
Pasadena, CA 91101

Engineering Division
California Institute of Technology
Pasadena, CA 91109

Professor H. Liepmann
Department of Aeronautics
California Institute of Technology
Pasadena, CA 91109

Science and Technology Division
Library of Congress
Washington, DC 20540

Library
Jet Propulsion Laboratory
4800 Oak Grove Drive
Pasadena, CA 91103

Mr. L. I. Chasen, MGR-MSD Lib.
General Electric Company
Missile and Space Division
P. O. Box 8555
Philadelphia, PA 19104

Technical Library
Naval Missile Center
Point Mugu, CA 93041

Professor S. Bogdonoff
Gas Dynamics Laboratory
Forrestal Campus
Princeton University
Princeton, NJ 08540

Professor S. I. Cheng
Gas Dynamics Laboratory
Forrestal Campus
Princeton University
Princeton, NJ 08540

Professor J. H. Clarke
Division of Engineering
Brown University
Providence, RI 02912

Professor J. T. C. Liu
Division of Engineering
Brown University
Providence, RI 02912

Professor L. Sirovich
Department of Applied Mathematics
Brown University
Providence, RI 02912

Dr. P. K. Dai (R1/2178)
TRW Systems Group, Inc.
One Space Park
Redondo Beach, CA 90278

Redstone Scientific Information Center
Chief, Document Section
Army Missile Command
Redstone Arsenal, AL 35809

Library
National Bureau of Standards
Washington, DC 20234

Professor M. Lessen
Department of Mechanical Engineering
River Campus Station
The University of Rochester
Rochester, NY 14627

Editor, Applied Mechanics Review
Southwest Research Institute
8500 Culebra Road
San Antonio, TX 78206

Dr. H. Yoshihara
Mail Zone 630-00
General Dynamics-CONVAIR
P. O. Box 1128
San Diego, CA 92112

Library and Information Services
General Dynamics-CONVAIR
P. O. Box 1128
San Diego, CA 92112

Office of Naval Research
San Francisco Area Office
760 Market Street, Room 447
San Francisco, CA 94102

Mr. Tom Brundage
Defense Advanced Research Projects Agency
Research and Development Field Unit
APO 146, Box 271
San Francisco, CA 96246

Library
The Rand Corporation
1700 Main Street
Santa Monica, CA 90401

Department Librarian
Department of Aeronautics and Astronautics
University of Washington
Seattle, WA 98105

Professor M. van Dyke
Department of Aeronautics and Astronautics
Stanford University
Stanford, CA 94305

Director of Research (Code RR)
National Aeronautics and Space Administration
600 Independence Avenue, S.W.
Washington, DC 20546

Professor K. Karamcheti
Department of Aeronautics and Astronautics
Stanford University
Stanford, CA 94305

Dr. R. J. Hakkinen
Department 222
McDonnell Douglas Corporation
P. O. Box 516
St. Louis, MO 63166

Engineering Library
Department 218, Building 101
McDonnell Douglas Corporation
P. O. Box 516
St. Louis, MO 63166

Dr. Roger P. Heinisch
Honeywell, Inc.
Systems and Research Division - Aerospace Defense Group
2345 Walnut Street
St. Paul, MN 55113

Professor R. G. Stoner
Department of Physics
Arizona State University
Tempe, AZ 85721

The Library
Institute of Aerospace Studies
University of Toronto
Toronto 5, Canada

Dr. S. M. Yen
Coordinated Science Laboratory
University of Illinois
Urbana, IL 61801

Office of Naval Research
Code 438
Arlington, VA 22217 (3 copies)

Office of Naval Research
Code 421
Arlington, VA 22217

Office of Naval Research
Code 411
Arlington, VA 22217

Office of Naval Research
Code 1021P (ONRL)
Arlington, VA 22217 (6 copies)

Mr. W. Koven (AIR 320)
Naval Air Systems Command
Washington, DC 20361

Mr. R. Siewert (AIR 320D)
Naval Air Systems Command
Washington, DC 20361

Technical Library Division (AIR 604)
Naval Air Systems Command
Washington, DC 20361

SEA 03512
Naval Sea Systems Command
Washington, DC 20362

SEA 09G3
Naval Sea Systems Command
Washington, DC 20362

Dr. Harvey R. Chaplin
Code 16
Naval Ship Research & Dev. Center
Bethesda, MD 20084

Code 5643
Naval Ship Research & Dev. Center
Bethesda, MD 20084

Code 1800
Naval Ship Research & Dev. Center
Bethesda, MD 20084

Chief of Research & Development
Office of Chief of Staff
Department of the Army
Washington, DC 20310

Mr. Robert A. Moore
Deputy Director, Tactical Technology Office
Defense Advanced Research Projects Agency
1400 Wilson Boulevard
Arlington, VA 22209

Dr. A. L. Slafkosky
Scientific Advisor
Commandant of the Marine Corps
(Code AX)
Washington, D. C. 20380

Science and Technology Division
Library of Congress
Washington, D. C. 20540

Director of Research (Code RR)
National Aeronautics and Space
Administration
600 Independence Avenue, S. W.
Washington, D. C. 20546

Library
National Bureau of Standards
Washington, D. C. 20234

National Science Foundation
Engineering Division
1800 G Street, N. W.
Washington, D. C. 20550

Director
Weapons Systems Evaluation Group
Washington, D. C. 20305

Bell Telephone Laboratories, Inc.
Whippany Laboratories
Whippany, NJ 07981

Librarian
Naval Surface Weapons Center
White Oak Laboratory
Silver Spring, MD 20910

Dr. J. M. Solomon
Naval Surface Weapons Center
White Oak Laboratory
Silver Spring, MD 20910

Chief of Aerodynamics
AVCO Corporation
Missile Systems Division
201 Lowell Street
Wilmington, MA 01887

Research Library
AVCO Corporation
Missile Systems Division
201 Lowell Street
Wilmington, MA 01887

AFAPL (APRC)
AB
Wright Patterson AFB, OH 45433

Mr. R. Feldhuhn
Naval Surface Weapons Center
White Oak Laboratory
Silver Spring, MD 20910

Dr. Donald J. Harney
AFFDL/FX
Wright Patterson AFB, OH 45433

Professor Stanley Rubin
Polytechnic Institute of New York
Department of Aerospace Engineering
and Applied Mechanics
Farmingdale, NY 11735

Mr. B. H. Little, Jr.
Dept. 72-74, Zone 369
Lockheed-Georgia Company
Marietta, GA 30061

Mr. J. Marshall
Code 4063
Naval Weapons Center
China Lake, CA 93555